

METHODODOLOGY ARTICLE

Bayesian uncertainty analysis for complex systems biology models: emulation, global parameter searches and evaluation of gene functions.

Ian Vernon^{1*}, Junli Liu^{2†}, Michael Goldstein¹, James Rowe³, Jen Topping² and Keith Lindsey²

Abstract

Background: Many mathematical models have now been employed across every area of systems biology. These models increasingly involve large numbers of unknown parameters, have complex structure which can result in substantial evaluation time relative to the needs of the analysis, and need to be compared to observed data of various forms. The correct analysis of such models usually requires a global parameter search, over a high dimensional parameter space, that incorporates and respects the most important sources of uncertainty. This can be an extremely difficult task, but it is essential for any meaningful inference or prediction to be made about any biological system. It hence represents a fundamental challenge for the whole of systems biology.

Results: Bayesian statistical methodology for the uncertainty analysis of complex models is introduced, which is designed to address the high dimensional global parameter search problem. Bayesian emulators that mimic the systems biology model but which are extremely fast to evaluate are embedded within an iterative history match: an efficient method to search high dimensional spaces within a more formal statistical setting, while incorporating major sources of uncertainty. The approach is demonstrated via application to a model of hormonal crosstalk in Arabidopsis root development, which has 32 rate parameters, for which we identify the sets of rate parameter values that lead to acceptable matches between model output and observed trend data. The multiple insights into the model's structure that this analysis provides are discussed. The methodology is applied to a second related model, and the biological consequences of the resulting comparison, including the evaluation of gene functions, are described.

Conclusions: Bayesian uncertainty analysis for complex models using both emulators and history matching is shown to be a powerful technique that can greatly aid the study of a large class of systems biology models. It both provides insight into model behaviour and identifies the sets of rate parameters of interest.

Keywords: parameter search; kinetic models; emulation; Bayesian uncertainty analysis; Arabidopsis; root development; hormonal signalling

Background

Fundamental challenges facing systems biology

Recent advances in genome sequencing techniques, a variety of 'omic' techniques and bioinformatic analyses, have led to an explosion of systems-wide biological data. Thus, identification of molecular components at the genome scale based on biological data has become possible. However, a major challenge in biology is to analyse and predict how functions in cells emerge from interactions between molecular com-

ponents. Computational and mathematical modelling provide compelling tools to study the nonlinear dynamics of these complex interactions [1]. A particular example is kinetic modelling, in which the kinetics of each biological reaction are described in accordance with the corresponding biological process, and the properties of the whole system are described using differential equations: a common tool for analysing biological systems [2–4].

A critical problem found in the mathematical modelling of many complex biological systems, which is of particular severity in kinetic modelling, is that the models often contain large numbers of uncertain parameters (a common type being reaction rate param-

*Correspondence: i.r.vernon@durham.co.uk

¹Department of Mathematical Sciences, Durham University, South Road, DH1 3LE, Durham, UK

Full list of author information is available at the end of the article

[†]Joint corresponding author: junli.liu@durham.ac.uk

eters). In most cases, such kinetic parameters cannot be directly measured as experiments typically measure concentrations rather than rates. Even when such parameters can be measured ‘directly’, this is usually in experimental conditions that are significantly different from the cellular environment we wish to study. Therefore, we have to compare the mathematical model’s outputs with experimental observations, often in the form of measured concentrations and trends, and determine which values of the input or rate parameters will achieve an acceptable match between model and reality. This involves consideration of several sources of uncertainty including observation error, biological variability and the tolerance we place on the model’s accuracy, known as the model discrepancy. It is vital that we perform a *global* parameter search for *all* input parameter settings that achieve an acceptable match. This is because a single solution for the rate parameter values may suggest certain biological implications and give particular predictions for future experiments, both of which could be gravely misleading were we to explore the parameter space further and find several alternative solutions that give radically different implications and predictions. This is a mistake that is disturbingly common.

Unfortunately, performing global parameter searches over high dimensional spaces can be extremely challenging for several reasons, most notably: (a) the complex structure of the model and hence the complex way it imposes constraints on the parameters, (b) the substantial model evaluation time relative to the needs of the analysis, (c) the need for a careful assessment of an “acceptable match” that incorporates appropriately all the complexities and uncertainties of the comparison between the model and the real system, and (d) high dimensional spaces, being extremely large, require *vast* numbers of model evaluations to explore. For example, some spatial models of root development [5] require at least several minutes for a single evaluation. It is worth considering how large high dimensional spaces are: were we just to evaluate the model in question at the corners of the initial input space, in say 32 dimensions, we would require $2^{32} \simeq 4.3$ billion evaluations, which would take approximately 136 years if the model took 1 second per evaluation. However, global parameter searches are essential for any meaningful inference or prediction to be made about the biological system. Therefore this represents a fundamental challenge for the whole of systems biology. This article describes practical methodology to address this problem, based on Bayesian statistics methodology for the uncertainty analysis of complex models [6–9].

Bayesian emulation and uncertainty analysis

The issues surrounding the analysis of complex models under uncertainty, and specifically the global pa-

rameter search problem, are not unique to systems biology, and have been encountered in many different scientific disciplines. An area of Bayesian statistics has arisen to meet the demand of such analyses. This area, sometime referred to as the uncertainty analysis of computer models, centres around the construction of Bayesian emulators [6–9]. An emulator is a statistical construct that mimics the scientific model in question, providing predictions of the model outputs with associated uncertainty, at as yet unevaluated input parameter settings. The emulator is however, extremely fast to evaluate [10]. It provides insight into the model’s structure and, thanks to its speed, it can be used to help perform the global parameter search far more efficiently than approaches that just use the comparatively slow scientific model itself (for examples see [6, 8, 11–14]).

Many analyses and corresponding parameter searches still fail because an appropriate measure of an acceptable match between model and reality is not defined. This can lead to the use of badly behaved objective functions that do not properly capture the desired match criteria, and which are often harder to explore in high dimensions, due to increased numbers of ridges, spikes and local minima. The Bayesian emulation methodology we introduce naturally incorporates more detailed statistical models of the difference between the model outputs and the observed data, which allow the inclusion of important sources of uncertainty such as observational error and model discrepancy, the later being the upfront acknowledgement of the limitations of the current model. Various structures of increasing complexity are available for the representation of these uncertainties, depending on the requirements and importance of the study (see [6, 15–18] for examples and discussion).

It is worth noting that due to their speed, the use of emulators would greatly improve the efficiency of many forms of analysis that a modeller may wish to perform, e.g. for a fully Bayesian MCMC analysis [9, 19, 20] or for more direct global parameter searches such as [21]. However for high dimensional models, the particular strategy chosen for a parameter search is vital. Many approaches struggle due to being trapped in local minima (of which there may be many) or because they chase the scientifically spurious best match parameter setting. Here, we describe an efficient global parameter search method known as Bayesian history matching, which has proved very successful across a wide range of scientific disciplines including cosmology [6, 7, 15, 22–24], epidemiology [11, 25], oil reservoir modelling [8, 26–28], climate modelling [12] and environmental science [16]. It utilises Bayesian emulators to reduce efficiently the input parameter space

in iterations or waves, by identifying regions that are implausible as matches to the observed data, with the objective of identifying all acceptable input parameter settings. It is a careful approach that avoids many of the traps of common parameter search techniques.

Hormonal crosstalk network in Arabidopsis root development

Understanding how hormones and genes interact to coordinate plant growth is a major challenge in developmental biology. The activities of auxin, ethylene and cytokinin depend on the cellular context and exhibit either synergistic or antagonistic interactions. Previously, three of our authors developed a hormonal crosstalk network for a single Arabidopsis cell by iteratively combining modelling with experimental analysis [29]. Kinetic modelling was used to analyse how such a network regulates auxin concentration in the Arabidopsis root, by controlling the relative contribution of auxin influx, biosynthesis and efflux; and by integrating auxin, ethylene and cytokinin signalling [29]. Although some of the parameters in the model were based on experimental data, most parameters were chosen in an ad hoc way, by adjusting them to fit experimental data. Conditional on those somewhat ad hoc choices, it was shown that the hormonal crosstalk network quantitatively describes how the three hormones (auxin, ethylene, and cytokinin) interact via POLARIS peptide (PLS) [30, 31] to regulate plant root growth [29].

In this work we demonstrate the power of the Bayesian emulation methodology by applying it to the hormonal crosstalk network in Arabidopsis root development. Specifically, we explore the model's 32-dimensional parameter space, and identify the set of all acceptable matches between model outputs and experimental data, taking into account major sources of uncertainty. This provides much insight into the model's structure and the constraints imposed on the rate parameters by the current set of observed data. We apply the methodology to a second, competing model, and hence are able to investigate gene functions robustly. As an example, our analysis suggest that, in the context of the hormonal crosstalk network, POLARIS peptide (PLS) must have a role in positively regulating auxin biosynthesis.

The paper is organised as follows. In the Methods section we begin by defining a simple 1-dimensional toy model that we use to illustrate our definitions and to demonstrate the three main parts of the Bayesian methodology: linking the model to reality, Bayesian emulation, and history matching. In the Results and Discussion section we describe in detail the application of this methodology to the full 32 dimensional Arabidopsis model, and discuss the relevant insights and biological implications obtained.

Methods

Simple 1-dimensional exponential example

Here we introduce a simple 1-dimensional exponential toy model example which we will use to illustrate our definitions of all the parts of a typical systems biology analysis, for example, the model, the input or rate parameters, observations with errors, model discrepancy, Bayesian emulators, implausibility measures and history matching. Specifically, this 1-dimensional example will be used throughout this Methods section to demonstrate each of the three main parts of our approach:

- Linking the model to reality
- Bayesian Emulation
- History matching: a global parameter search

Say we are interested in the concentration of a chemical which evolves in time. We represent this concentration as $f_t(x)$ where x is, for example, a reaction rate parameter and t is time. We model $f_t(x)$ with the differential equation:

$$\frac{df_t(x)}{dt} = x f_t(x) \quad (1)$$

which in this case we can solve precisely to give

$$f_t(x) = f_0 \exp(xt) \quad (2)$$

We will temporarily assume the initial conditions are $f_0 = f_{t=0}(x) = 1$. The system runs from $t = 0$ to $t = 5$ and we are at first interested in the value of $f_t(x)$ at $t = 3.5$. This mathematical model features an input or rate parameter x , which we wish to learn about. We do this using a measurement of the real biological system at $t = 3.5$ which we denote z , which corresponds to, but is not the same as, the model output $f_{t=3.5}(x)$. Note that usually, for models of realistic complexity, we would not have the analytic solution for $f_t(x)$ given by equation (2). Instead we would resort to a numerical integration method to solve equation (1) that might require significant time for one model evaluation, ranging from less than a second to hours, days or even weeks, depending on the full complexity of the model [6, 12]. Such a computational cost, for a single evaluation of the model, means that a full global parameter search is computationally infeasible, especially when the model has many rate parameters and therefore a high dimensional input space, which may require vast numbers of evaluations to explore fully.

We typically begin the analysis by exploring the model's behaviour for several different values of the unknown rate or input parameter x . Figure 1 (left panel), shows five evaluations of the model $f_t(x)$ for different values of x between $x = 0.1$ and 0.5 , coloured red to

purple respectively, with time on the x-axis. The measurement of the system is denoted z , and is represented as the black point in figure 1, with $\pm 3\sigma_e$ error bars representing observational error, defined precisely below. This measurement was made at $t = 3.5$ shown as the vertical dashed line. The most important questions for the biologist at this point are: can the model match the observed data z at all, and if so, what is the entire set of input parameter choices that give rise to acceptable matches between model output and observed data? Figure 1 (right panel) represents this question as it now shows only $f_{t=3.5}(x)$ but now represented purely as a function of the input parameter x on the x-axis, with the red to purple points consistent with those in the left panel. The observed data z is now represented as the solid black horizontal line, with the $\pm 3\sigma_e$ error bars as the horizontal black dashed lines. We see that there will be acceptable values of x approximately between 0.3 and 0.35.

For a general complex model $f_t(x)$, that possesses a large number of input or rate parameters and possibly several outputs, a full analysis of the model's behaviour encounters the following issues:

- 1 When comparing the model to observed data from the real biological system, an adequate statistical description of the link between model and reality, covering all major uncertainties, is required.
- 2 For complex models, the time taken to evaluate the model numerically is so long that an exhaustive exploration of the model's behaviour is not feasible.
- 3 The appropriate scientific goal should be to identify *all* locations in input parameter space that lead to acceptable fits between model and data, and not just find the location of a single good match.

Methods to address these three fundamental issues are described in the next three sections.

Model Discrepancy and Linking the model to reality

Most systems biology models are developed to help explain and understand the behaviour of corresponding real world biological systems. An essential part of determining whether such models are adequate for this task is the process of comparing the model to experimental data. As a comparison of this kind involves several uncertainties that cannot be ignored, it is therefore vital to develop a clearly defined statistical model for the link between systems biology model $f(x)$ and reality z . This allows for a meaningful definition of an 'acceptable' match between a model run and the observed data. Here we describe a simple yet extremely useful statistical model for the link between the biological model and reality, that has been successfully

applied in a variety of scientific disciplines, for example climate, cosmology, oil reservoir modelling and epidemiology [6, 8, 11, 12].

The most recognisable source of uncertainty is that of observational or experimental error. We represent the uncertain quantities of interest in the real biological system as the vector y , which we will measure with a vector of errors e to give the vector of observations z , such that

$$z = y + e \quad (3)$$

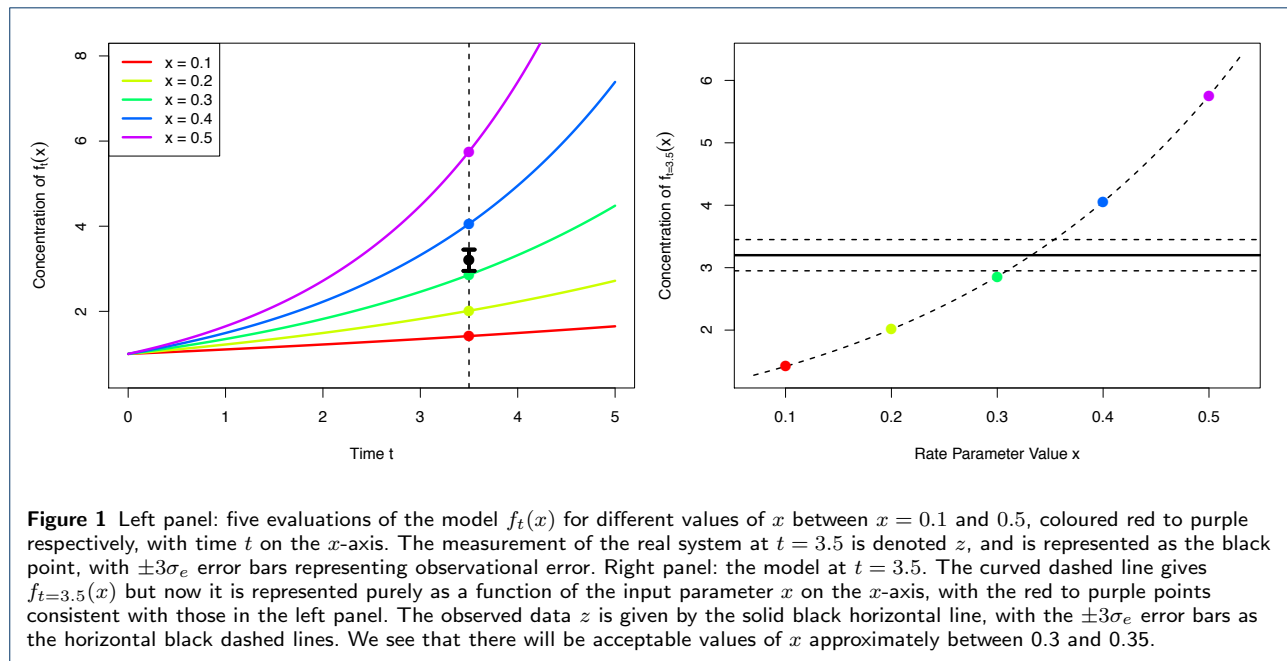
where we represent the errors as additive, although more complex forms could be used. Note that z , y and e here represent vectors of random quantities, which will reduce to scalar random quantities if there is only one quantity of interest. A common specification [6] that we will employ here is to judge the errors to be independent from y , and unbiased with expectation $E(e) = 0$ and, for the scalar case, $\text{Var}(e) = \sigma_e^2$.

An important distinction to make is between the model of the biological system, represented as the vector $f(x)$, and the system itself y . We represent the difference between these using a *model discrepancy* term as follows. Even were we to evaluate the model $f(x)$ at its best possible choice of input x^* , the output $f(x^*)$ would still not be in agreement with the real biological system value y , due to the many simplifications and approximations of the model. Hence we state that:

$$y = f(x^*) + \epsilon \quad (4)$$

where the ϵ is the model discrepancy: a vector of uncertain quantities that represents directly the difference between the model and the real system. Again we treat y , f , x^* and ϵ as vectors of random quantities. A simple and popular specification [6] would be to judge that ϵ is independent of $f(x^*)$, x^* and e , with $E(\epsilon) = 0$ and, in the scalar case, $\text{Var}(\epsilon) = \sigma_\epsilon^2$. In a multivariate setting, where $f(x)$ describes a vector of outputs (for example, with each output labelled by time t), the vector ϵ may have an intricate structure, possessing non-zero covariances between components of ϵ . This could capture the related deficiencies of the model across differing time points. Various structures of increasing complexity are available (for examples see [6, 8, 9]), along with methods for specification of their components [6, 16].

While the explicit inclusion of the model discrepancy term ϵ is unfamiliar, it is now standard practice in the statistical literature for complex models [7, 9, 17, 32]. Furthermore, any analysis performed without such a term has to be conditioned with the statement "given the model is a perfect representation of reality for some value of the inputs x ", a statement that is rarely true.



We can specify probabilistic attributes of ϵ a priori, or learn about them by comparing to observed data. For direct specification, there are often various simple experiments that can be performed on the model itself to obtain assessments of σ_ϵ and other aspects if necessary. For example, often models are run from exact initial conditions, so performing a set of exploratory model evaluations with the initial conditions appropriately perturbed would provide a lower bound on σ_ϵ . See [16] where several such assessment methods are demonstrated, for more details.

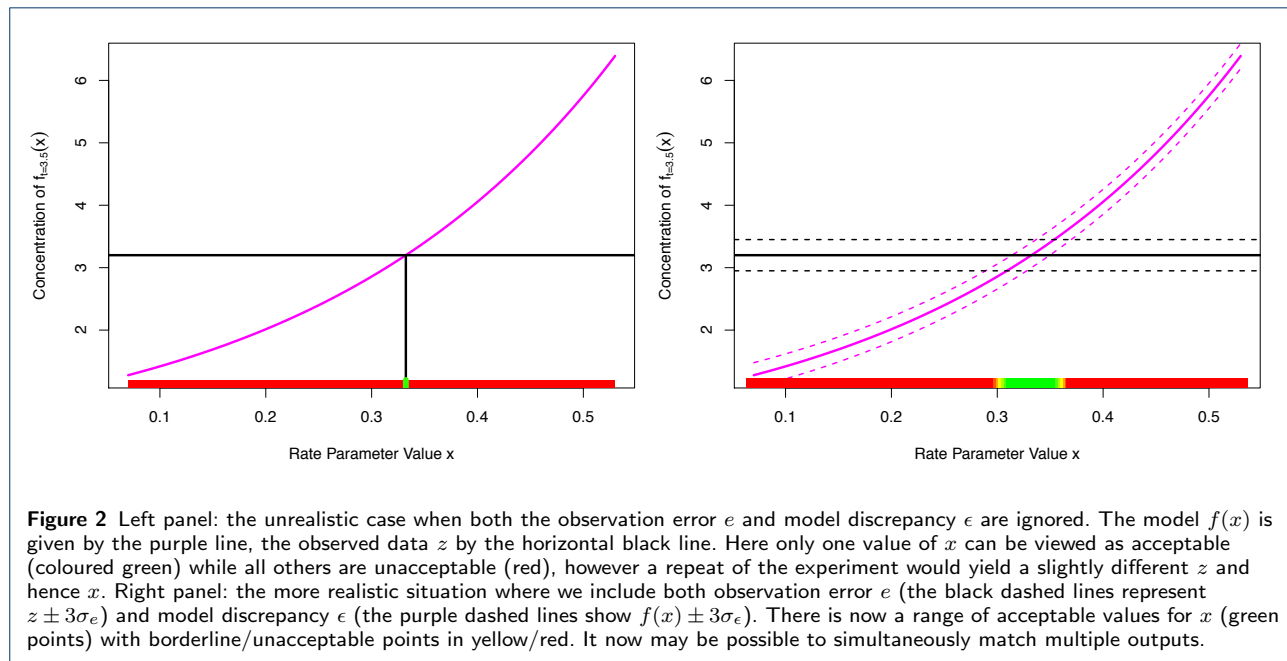
1-dimensional example

Figure 2 (left panel) shows the case for the simple 1-dimensional exponential example model when both the observation error e and model discrepancy ϵ are ignored. The model $f(x)$ is given by the purple line, while the observed data z is given by the horizontal black line. Here only one value of x can be viewed as acceptable (coloured green) while all others are unacceptable (red). This particular value of x is not unique in that if we were to perform the measurement again, due to measurement error we would get a different value for z and hence for x . More importantly, if the model had a second output, say corresponding to a different time, that also depended on the same input x , we would be extremely unlikely to be able to match both outputs to their measurements as we would have to obtain exact matches simultaneously for precisely the same value of x . Inferences and predictions about the biological system made from this case, using this value of x are not trustworthy.

Figure 2 (right panel) shows the far more realistic situation where we include both observation error e (the black dashed lines represent $z \pm 3\sigma_e$) and model discrepancy ϵ (the purple dashed lines show $f(x) \pm 3\sigma_\epsilon$). As we have taken into account both major types of uncertainty there is now a range of acceptable values for x (green points) with borderline/unacceptable points in yellow/red. If we were to consider additional outputs of the model, we still have a chance to match them simultaneously to data for a subset of the currently acceptable points. If on the other hand we cannot find any acceptable points x even given the uncertainties represented by e and ϵ , then we can state that the model is inconsistent with the observed data and therefore most likely based on incorrect biological principles. Further, inclusion of the observation error and model discrepancy terms often aids a global parameter search as they tend to smooth the likelihood surface (or comparable objective function), making it both easier to explore while simultaneously more robust. They also help reduce the temptation to chase the scientifically meaningless global minimum, such as the lone green point in figure 2 (left panel), instead suggesting that the identification of a set of acceptable input points is the appropriate goal for such a search (see the green points in figure 2 (right panel)).

Bayesian emulation of systems biology models

Many complex mathematical models have been developed and employed within the area of systems biology. Often these models have high dimensional input spaces



in that they possess several input parameters, for example reaction rate parameters, that must be specified in order to evaluate the model. We represent the list of such inputs as the vector x , with individual inputs as x_k with $k = 1, \dots, d$. The model may have any number of outputs, denoted as the vector $f(x)$, with individual outputs as $f_i(x)$ with $i = 1, \dots, q$, the behaviour of which we want to investigate, possibly comparing some of these to observed data. For example, the index i may label the different times we are interested in, or the different chemical outputs of the model, or both. Most models are complex enough that they require numerical integration methods to solve, and hence take appreciable time to evaluate. This evaluation time can range anywhere from less than a second to minutes, hours or even days for highly sophisticated models: our approach is applicable in any of these cases, and adds more value as the dimensionality and evaluation time of the model increases.

A Bayesian emulator is a fast, approximate mimic of the full systems biology model. It gives insight into the structure of the model's behaviour and can be used instead of the model in many complex calculations. The emulator gives a prediction of what the model's output $f(x)$ will be at a yet to be evaluated input point x , and additionally provides an associated uncertainty for that prediction (these are often expressed as posterior distributions, or simply expectations and variances in some cases). Critically an emulator is extremely fast to evaluate as it only requires a few matrix multiplications, and hence can be used to explore the input

space more fully, as for example in a global parameter search.

A popular choice for the Bayesian emulator for model $f(x)$, which has individual outputs $f_i(x)$, $i = 1 \dots q$, is structured as follows:

$$f_i(x) = \sum_j \beta_{ij} g_{ij}(x_{A_i}) + u_i(x_{A_i}) + w_i(x) \quad (5)$$

where the active variables x_{A_i} are a subset of the inputs x that are most influential for output $f_i(x)$. The first term on the right hand side of the emulator equation (5) is a regression term, where g_{ij} are known deterministic functions of x_{A_i} , a common choice being low order polynomials, and β_{ij} are unknown scalar regression coefficients. The second term, $u_i(x_{A_i})$ is a Gaussian process^[1] over x_{A_i} which means that if we choose a finite set of inputs $\{x_{A_i}^{(1)}, \dots, x_{A_i}^{(s)}\}$, the uncertain outputs $u_i(x_{A_i}^{(1)}), \dots, u_i(x_{A_i}^{(s)})$ will have a multivariate normal distribution with a covariance matrix constructed from an appropriately chosen covariance function, for example:

$$\text{Cov}(u_i(x_{A_i}), u_i(x'_{A_i})) = \sigma_{u_i}^2 \exp \left\{ -\frac{\|x_{A_i} - x'_{A_i}\|^2}{\theta_i^2} \right\} \quad (6)$$

where $\sigma_{u_i}^2$ and θ_i are the variance and correlation length of $u_i(x_{A_i})$ which must be specified [6]. The third

^[1]Or in a less fully specified version, a weakly second order stationary stochastic process.

term $w_i(x)$ is a nugget, a white noise process uncorrelated with β_{ij} , $u_i(x_{A_i})$ and itself such that

$$\text{Cov}(w_i(x), w_i(x')) = \begin{cases} \sigma_{w_i}^2 & \text{if } x = x' \\ 0 & \text{otherwise} \end{cases} \quad (7)$$

with expectation zero and $\text{Var}(w_i(x)) = \sigma_{w_i}^2$, that represents the effects of the remaining inactive input variables [6].

The emulator, as given by equation (5), possesses various desirable features. The regression term, given by $\sum_j \beta_{ij} g_{ij}(x_{A_i})$, is often chosen to represent say a third order polynomial in the active inputs. This would attempt to mimic the large scale global behaviour of the function $f_i(x)$, and in many cases, will capture a large proportion of the model's structure^[2]. The second term $u_i(x_{A_i})$, the Gaussian process, mimics the local behaviour of $f_i(x)$ and specifically its local deviations from the third order polynomial given by the regression terms. We can choose the list of active inputs x_{A_i} using various statistical techniques for example, classical linear model fitting criteria such as AIC or BIC [6]. A list of say p active inputs for a particular output $f_i(x)$ means that we have reduced the input dimension from d to p dimensions, which can result in large efficiency gains. The small remaining effect of the inactive inputs is captured by the third term $w_i(x)$ in equation (5).

We proceed by performing an initial set of carefully chosen model evaluations, often picked to be 'space filling', i.e. well spread out over the input space. For example we may use a maximin latin hypercube design, an approximately orthogonal design which attempts to ensure there are no large holes in-between the run locations (see figure 3 and [33–35]). An n point latin hypercube design is created by dividing the range of each input into n sub-intervals, and placing points to ensure there is only ever one point in each sub-interval (this can be done using the `lhs()` function in R [36]). Many such latin hypercube designs are generated and the one with maximum minimum distance between points is chosen.

We then fit the emulator given by equation (5) to the set of model runs using our favourite statistical tools, guided by expert judgement. Specifically we would prefer a fully Bayesian approach if we required full probability distributions [9], and a Bayes Linear approach [37, 38], which we will describe below, if we required purely expectations, variances and covariances

^[2]It is worth noting that reasonably accurate emulators can often be constructed just using regression models, for example using the `lm()` function in R. This can be a sensible first step, before one attempts the construction of a full emulator of the form given in equation (5).

of $f(x)$. We make certain pragmatic choices in the emulator construction process, for example, while we keep the regression coefficients β_{ij} uncertain, we may directly specify $\sigma_{u_i}^2$, $\sigma_{w_i}^2$ and θ_i a priori, or use suitable plugin estimates [6].

The emulators then provide an expectation and variance for the value of $f(x)$ at an unexplored input point x . We can test the emulators using a series of diagnostics, for example checking their prediction accuracy over a new batch of runs [39]. See [10] for an introduction and [6, 7, 9] for detailed descriptions of emulator construction.

While there are several approaches to emulator construction, our preferred choice is to use Bayes Linear methods, which is a more tractable version of Bayesian statistics which requires a far simpler prior specification and analysis [37, 38]. It deals purely with expectations, variances and covariances of all uncertain quantities, and uses the following update equations to adjust our beliefs in the light of new data. Say we had performed an initial wave of n runs at input locations $x^{(1)}, x^{(2)}, \dots, x^{(n)}$ giving a column vector of model output values $D_i = (f_i(x^{(1)}), f_i(x^{(2)}), \dots, f_i(x^{(n)}))^T$, where i labels the model output. We obtain the adjusted expectation and variance for $f_i(x)$ at new input point x using:

$$\text{E}_{D_i}(f_i(x)) = \quad (8)$$

$$\text{E}(f_i(x)) + \text{Cov}(f_i(x), D_i) \text{Var}(D_i)^{-1} (D_i - \text{E}(D_i))$$

$$\text{Var}_{D_i}(f_i(x)) = \quad (9)$$

$$\text{Var}(f_i(x)) - \text{Cov}(f_i(x), D_i) \text{Var}(D_i)^{-1} \text{Cov}(D_i, f_i(x))$$

All quantities on the right hand side of equations (8) and (9) can be calculated from equations (5) and (6) combined with prior specifications for $\text{E}(\beta_{ij})$, $\text{Var}(\beta_{ij})$, $\sigma_{u_i}^2$, $\sigma_{w_i}^2$ and θ_i . Note that we could have used the entire collection of model outputs $D = \{D_1, D_2, \dots, D_q\}$ instead of just D_i in equations (8) and (9), if we had specified a more complex, multivariate emulator [40].

$\text{E}_{D_i}(f_i(x))$ and $\text{Var}_{D_i}(f_i(x))$ are used directly in the implausibility measures used for the global parameter searches described below.

1-dimensional example

We now demonstrate the construction of an emulator for the simple one dimensional exponential model. As there is only one output dimension, $f(x)$ is now a scalar, so we drop the i index from equations (5–9).

Figure 4 (left panel) shows output from such an emulator of the simple model defined by equation 1. We suppose that only $n = 5$ runs of the model have been performed at the locations $x^{(j)} = 0.1, 0.2, 0.3, 0.4, 0.5$,

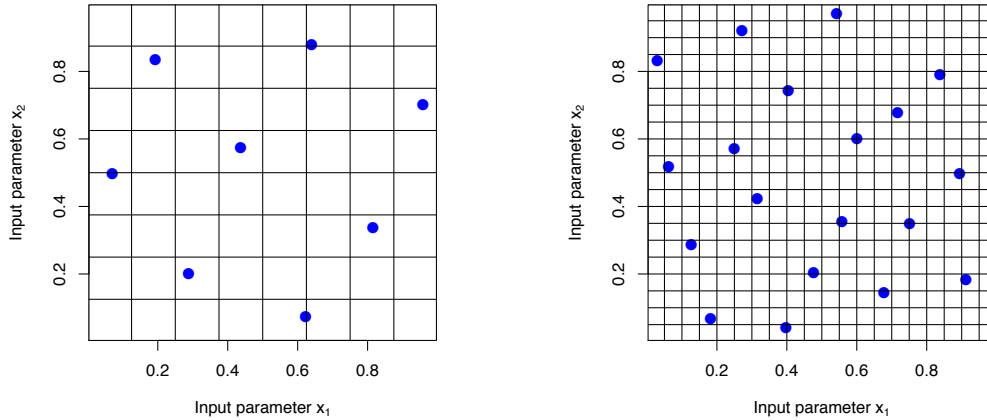


Figure 3 Maximum minimum distance Latin hypercube designs of size $n = 8$ (left panel) and $n = 20$ (right panel). The blue points represent locations in rate or input parameter space where we would run the full systems biology model. These designs are both space filling and approximately orthogonal, both desirable features for fitting emulators. Note that the construction process of a latin hypercube ensures that there is a blue point within each of the n subintervals of both inputs, ensuring excellent coverage.

which are shown as the purple points (these are the same as the five coloured points in figure 1). We therefore have the model output values

$$D = (f(x^{(1)}), f(x^{(2)}), \dots, f(x^{(5)}))^T \quad (10)$$

$$= (e^{0.1 \times 3.5}, e^{0.2 \times 3.5}, \dots, e^{0.5 \times 3.5})^T$$

where again the output of interest has $t = 3.5$.

We use a simplified form of the emulator given by equation (5), where we choose the polynomial terms $\beta_j g_j(x_A)$ to represent only a constant term β_0 . As we only have one input variable, there is no distinction between inactive and active variables so we also set $w(x)$ to zero, and hence the emulator equation (5) reduces to

$$f(x) = \beta_0 + u(x) \quad (11)$$

For simplicity we treat the constant term β_0 as known and hence set $\text{Var}(\beta_0) = 0$, and choose prior expectation $E(\beta_0) = \beta_0 = 3.5$, a value which we expect the function outputs to be approximately centred around. We specify the parameters in the covariance function for $u(x)$ given by equation (6) to be $\sigma_u = 1.5$ and $\theta = 0.14$ representing curves of moderate smoothness: this process will be discussed in more detail for the full Arabidopsis model.

All expectation, variance and covariance terms on the right hand side of equations (8) and (9) can now be

found using equations (11), (6) and (10), for example,

$$E(f(x)) = \beta_0 \quad (12)$$

$$\text{Var}(f(x)) = \sigma_u^2 \quad (13)$$

$$E(D) = (\beta_0, \dots, \beta_0)^T \quad (14)$$

while $\text{Cov}(f(x), D)$ is a row vector of length n with j th component

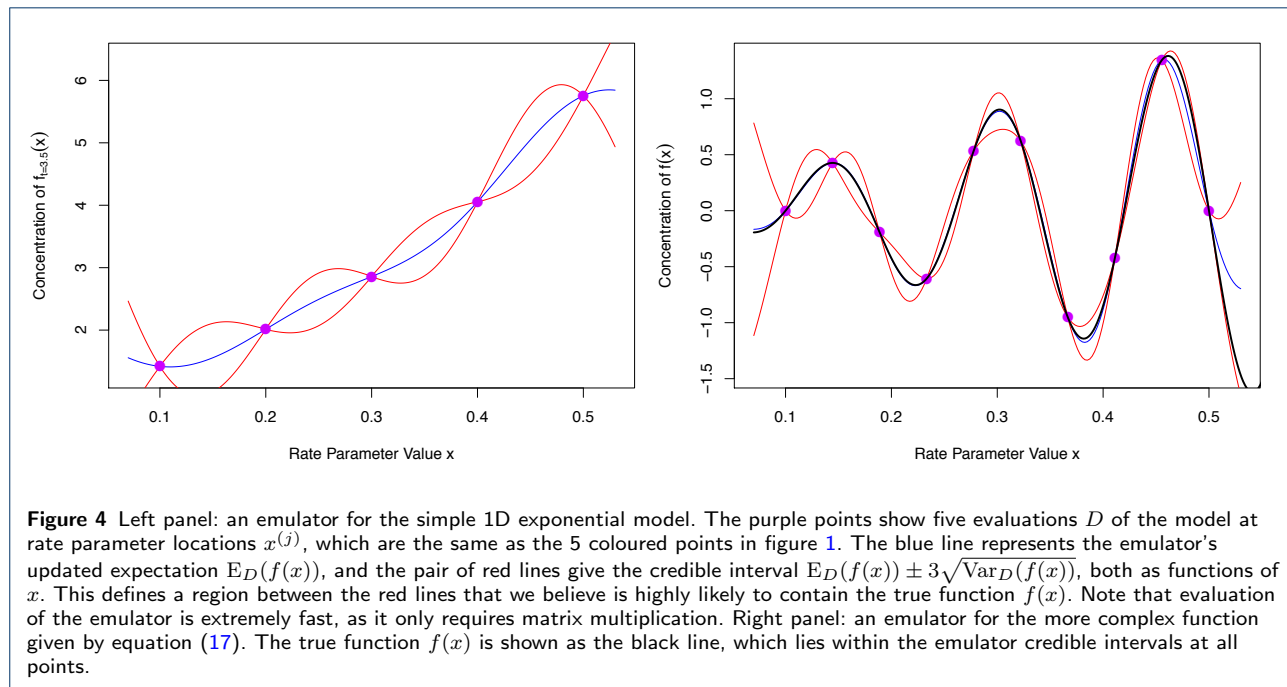
$$\begin{aligned} \text{Cov}(f(x), D)_j &= \text{Cov}(f(x), f(x^{(j)})) \quad (15) \\ &= \sigma_u^2 \exp \left\{ -\frac{\|x - x^{(j)}\|^2}{\theta^2} \right\} \end{aligned}$$

and similarly $\text{Var}(D)$ is an $n \times n$ matrix with (j, k) element

$$\begin{aligned} \text{Var}(D)_{jk} &= \text{Cov}(f(x^{(j)}), f(x^{(k)})) \quad (16) \\ &= \sigma_u^2 \exp \left\{ -\frac{\|x^{(j)} - x^{(k)}\|^2}{\theta^2} \right\} \end{aligned}$$

We can now calculate the adjusted expectation and variance $E_D(f(x))$ and $\text{Var}_D(f(x))$ from equations (8) and (9) respectively.

Figure 4 (left panel) shows $E_D(f(x))$ as a function of x as the blue line. We can see that it precisely interpolates the five known runs at outputs D , which is desirable as $f(x)$ is a deterministic function. The blue line also gives a satisfactory estimate of the true function $f(x) = \exp(3.5x)$. The red pair of lines give the credible interval $E_D(f(x)) \pm 3\sqrt{\text{Var}_D(f(x))}$ as a function of x . This defines a region between the lines that



we believe is highly likely to contain the true function $f(x)$. Another desirable feature of the emulator is that these credible intervals decrease to zero width at the five known run locations, as is appropriate for a deterministic function, as we precisely know the value of $f(x)$ there (and because we have no inactive variables). Therefore when x is close to a known run we are more certain about the possible values of $f(x)$, compared to when x is far from any such runs.

Figure 4 (right panel) shows an emulator as applied to a more complex 1-dimensional function. Here the true function is

$$f(x) = 3x \sin\left(\frac{5\pi(x-0.1)}{0.4}\right) \quad (17)$$

which has been simulated at only 10 input points evenly spread between $x^{(1)} = 0.1$ and $x^{(10)} = 0.5$. Here the prior emulator specifications were as in the previous example, but with $E(\beta_0) = 0$, $\sigma_u = 0.6$ and $\theta = 0.06$ allowing for functions with more curvature, centred around zero. As before the blue and red lines show $E_D(f(x))$ and $E_D(f(x)) \pm 3\sqrt{\text{Var}_D(f(x))}$ as functions of x . The true function $f(x)$ is given by the solid black line and it can be seen that it lies within the credible region for all x , only getting close to the boundary for $x > 0.5$. This demonstrates the power of the emulation process: with the use of only 10 points the emulator accurately mimics a reasonably complex function with five turning points. We will demonstrate the effectiveness of emulators in higher dimensions for the main Arabidopsis model example.

History matching: an efficient global parameter search

Bayesian emulation is very useful in a variety of situations. As emulators are extremely fast to evaluate, they can replace the original model in any larger calculation, for example when designing future experiments [41, 42]. They can also provide much structural insight into the behaviour of the model. One of the most important applications of emulation is to the problem of performing a global parameter search. In this section we describe a powerful iterative global search method known as history matching, which has been successfully employed in a variety of scientific disciplines [6, 8, 11, 12], including to models with substantial runtime for which the process of emulation is vital.

When confronting a systems biology model with observed data the following questions are typically asked:

- 1 Are there any input parameter settings that lead to acceptable matches between the model output and observed data?
- 2 If so, what is the full set \mathcal{X} that contains all such input parameter settings?

History matching is designed to answer these questions. It proceeds iteratively and employs *implausibility measures* to determine parts of the input space that can be discarded from further investigation.

We can ask the question: for an unexplored input parameter setting x , how far would the emulator's expected value for the individual function output $f_i(x)$ be from the corresponding observed value z_i before we

could deem it highly unlikely for $f_i(x)$ to give an acceptable match were we to evaluate the function at this value of x ? The implausibility measure $I_i(x)$ captures this concept, and is given by:

$$I_i^2(x) = \frac{(E_{D_i}(f_i(x)) - z_i)^2}{\text{Var}_{D_i}(f_i(x)) + \text{Var}(\epsilon_i) + \text{Var}(e_i)} \quad (18)$$

The numerator of equation (18) gives the distance between the emulator expectation $E_{D_i}(f_i(x))$ and the observation z_i , while the denominator standardises this quantity by all the relevant uncertainties regarding this distance: the emulator variance $\text{Var}_{D_i}(f_i(x))$, the model discrepancy variance $\text{Var}(\epsilon_i)$ and the observation error variance $\text{Var}(e_i)$. This structure is a direct consequence of equations (3) and (4). A large value of $I_i(x)$ for a particular x implies that we would be unlikely to obtain an acceptable match between $f_i(x)$ and z_i were we to run the model there. Hence we can discard the input x from the parameter search if $I_i(x) > c$, for some cutoff c . We may choose the cutoff c by appealing to Pukelsheim's 3-sigma rule [43], which states that for *any* continuous, unimodal distribution, 95% of its probability must lie within $\pm 3\sigma$, regardless of asymmetry or skew, suggesting that a choice of $c = 3$ could be deemed reasonable [6].

We can combine the implausibility measures $I_i(x)$ from several outputs in various simple ways, for example we could maximise over all outputs defining

$$I_M(x) = \max_{i \in Q} I_i(x) \quad (19)$$

where Q represents the collection of all outputs, or some important subset of them (often we will only emulate a small subset of outputs in early iterations). A more robust approach would be to consider the second or third maximum implausibility, hence allowing for some inaccuracy of the emulators [6]. Also, multivariate implausibility measures are available (see [6] for details), but these require a more detailed prior specification, for example this requires covariances between different components of e and ϵ .

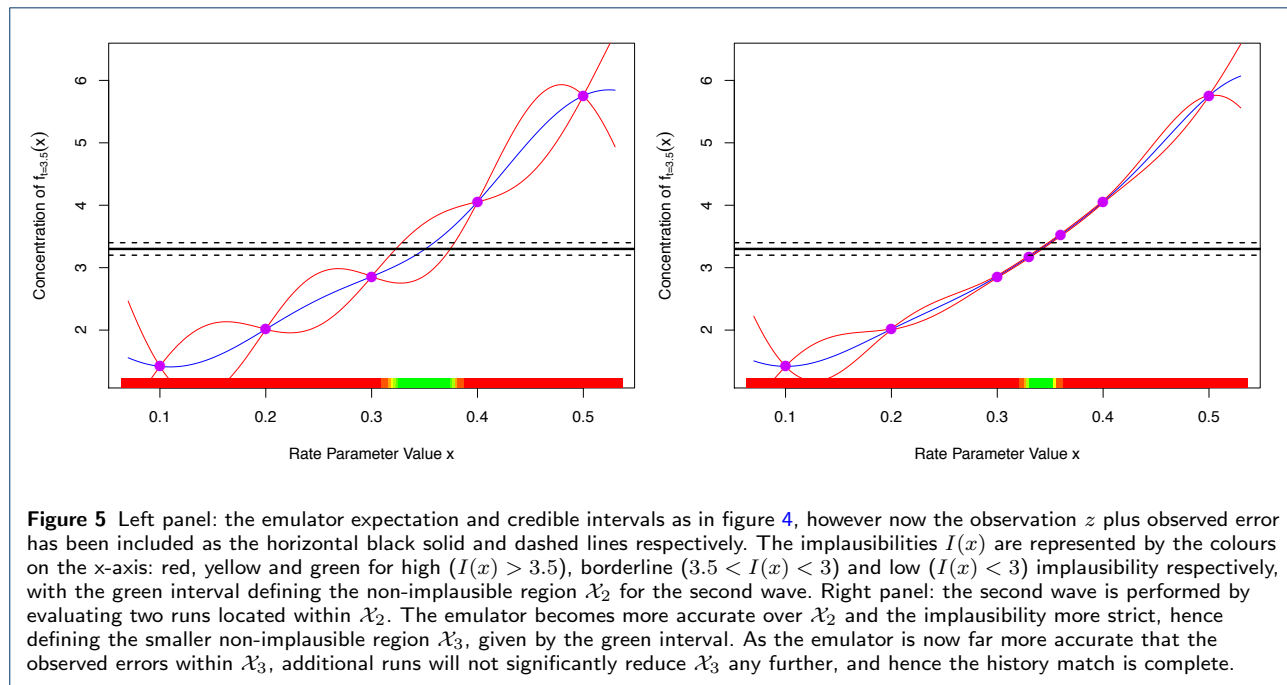
We proceed iteratively, discarding regions of the input parameter space in waves, refocussing our search on the remaining 'non-implausible' inputs at each wave. Prior to performing the k th wave, we define the current set of non-implausible input points as \mathcal{X}_k and the set of outputs that we considered for emulation in the previous wave as Q_{k-1} . We proceed according to the following algorithm.

- 1 Design and evaluate a well chosen set of runs over the current non-implausible space \mathcal{X}_k . e.g. using a maximin Latin hypercube with rejection [6].
- 2 Check to see if there are new, informative outputs that can now be emulated accurately (that were difficult to emulate well in previous waves) and add them to the previous set Q_{k-1} , to define Q_k .
- 3 Use the runs to construct new, more accurate emulators defined only over the region \mathcal{X}_k for each output in Q_k .
- 4 The implausibility measures $I_i(x)$, $i \in Q_k$, are then recalculated over \mathcal{X}_k , using the new emulators.
- 5 Cutoffs are imposed on the Implausibility measures $I_i(x) < c$ and this defines a new, smaller non-implausible volume \mathcal{X}_{k+1} which should satisfy $\mathcal{X} \subset \mathcal{X}_{k+1} \subset \mathcal{X}_k$.
- 6 Unless a) the emulator variances for all outputs of interest are now small in comparison to the other sources of uncertainty due to the model discrepancy and observation errors, or b) the entire input space has been deemed implausible, return to step 1.
- 7 If 6 a) is true, generate as large a number as possible of acceptable runs from the final non-implausible volume \mathcal{X} , sampled depending on scientific goal.

We then analyse the form of the non-implausible volume \mathcal{X} , the behaviour of model evaluations from different locations within it and the corresponding biological implications.

The history matching approach is powerful for several reasons:

- As we progress through the waves and reduce the volume of the region of input space of interest, we expect the function $f(x)$ to become smoother, and hence to be more accurately approximated by the regression part of the emulator $\beta_{ij}g_{ij}(x_{A_i})$, which is often composed of low order polynomials (see equation 5).
- At each new wave we have a higher density of points in a smaller volume and hence the Gaussian process term $u_i(x_{A_i})$ in the emulator will be more effective, as it depends mainly on the proximity of x to the nearest runs.
- In later waves the previously strongly dominant active inputs from early waves will have their effects curtailed, and hence it will be easier to select additional active inputs, unnoticed before.
- There may be several outputs that are difficult to emulate in early waves (perhaps because of their erratic behaviour in uninteresting parts of the input space) but simple to emulate in later waves once we have restricted the input space to a much smaller and more biologically realistic region.



1-dimensional example

We now demonstrate the history matching process as applied to the simple 1-dimensional exponential example. Figure 5 (left panel) shows the emulator expectation and credible intervals as in figure 4, however now the observation z plus observed error has been included as the horizontal black solid and dashed lines respectively. Here we have set the model discrepancy to zero ($\sigma_\epsilon = 0$) and reduced the size of the observation errors σ_e for clarity. Also given are the implausibilities $I(x)$ as represented by the colours on the x-axis: red, yellow and green for high ($I(x) > 3.5$), borderline ($3.5 < I(x) < 3$) and low ($I(x) < 3$) implausibility respectively.

The non-implausible space \mathcal{X}_1 at wave 1 is the full initial range of the rate parameter x , which is $0.075 < x < 5.25$. If we impose cutoffs of $I(x) < 3$ then this defines the wave 2 non-implausible space \mathcal{X}_2 as shown by the green region of the x-axis in figure 5 (left panel).

We then perform the second wave by designing a set of two more runs over \mathcal{X}_2 , reconstructing the emulator over this region, and recalculating the implausibility measure $I(x)$. The results of this second wave are shown in figure 5 (right panel). It can be seen that the emulator is now highly accurate over the \mathcal{X}_2 region and that the non-implausible region in green has been further reduced. As the emulator is now far more accurate than the corresponding observation error, we may stop the analysis with this wave as $\mathcal{X}_3 \simeq \mathcal{X}$, implying that further runs will do little to reduce the non-implausible region further. Note that providing we have enough

runs in each wave, we would often create new emulators at each wave, defined only over the current green non-implausible region [6], instead of updating emulators from previous waves, as in figure 5.

We now apply the techniques of Bayesian emulation and history matching to the full hormonal crosstalk network in Arabidopsis root development model.

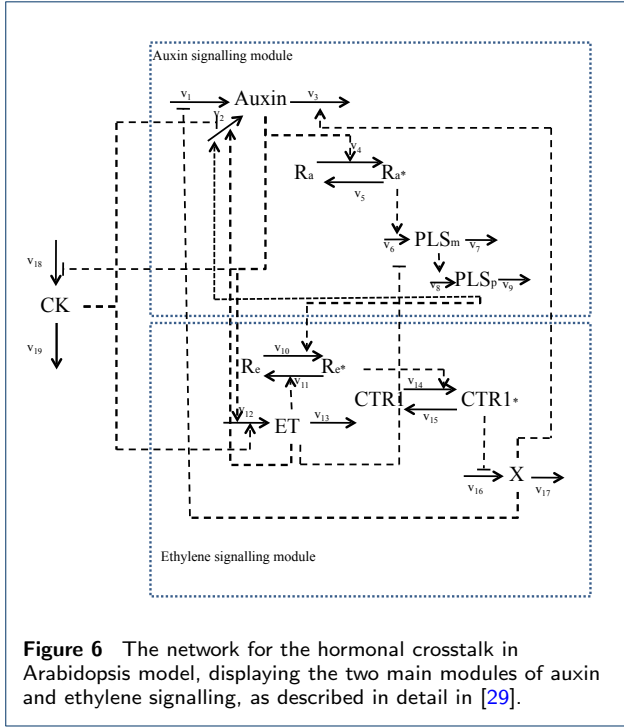
Results

Application to the hormonal crosstalk network in Arabidopsis root development model

We now describe the relevant features of the hormonal crosstalk in Arabidopsis root development model [29], in preparation for the application of the Bayesian emulation and history matching processes introduced above.

The hormonal crosstalk in Arabidopsis model was constructed on the basis of known molecular interactions and experimental evidence, and models the crosstalk between auxin, ethylene and cytokinin via the *PLS* gene in Arabidopsis root development. The network for the model is shown in figure 6 which displays the two main modules of auxin and ethylene signalling. A full description of the model, along with justifications of the various modelling choices employed, can be found in [29].

The mathematical representation of the Arabidopsis model, given in table 1, is a set of 15 ordinary differential equations that describe the evolution in time of 15 different biological quantities. Note the analogy with equation (1) describing the simple exponential



model. The Arabidopsis model requires the specification of 32 input or rate parameters before it can be evaluated: these are represented in table 1 as the parameters $(k_1, k_{1a}, \dots, k_{1veth})$. The rate parameter k_6 is an exception: it is a control parameter and is set to 0.3 to represent the wildtype and 0 to represent the *pls* mutant [29], and hence it will not be included in our parameter search, leaving 31 free parameters.

As we will compare the model output to data at equilibrium only [29], we can perform a substantial dimensional reduction of the input space. Referring to the model equations given in table 1, we see that at equilibrium the derivative on the left hand side of each equation will equal zero, and that the right hand side can hence be rearranged in terms of one less rate parameter. For example, the equation for $d[Ra]/dt$ becomes:

$$0 = -[Auxin][Ra] + \left(\frac{k_5}{k_4}\right) [Ra^*] \quad (20)$$

which depends only on the ratio of (k_5/k_4) . Hence data at equilibrium can inform only about the ratio (k_5/k_4) and cannot provide any constraint upon the original parameters k_4 and k_5 individually^[3]. We can therefore

^[3]It is worth noting that if the model was a stochastic model instead of a deterministic model, it may be possible to learn about the parameters individually, even at equilibrium, as discussed in chapter 1 of [44].

$$\begin{aligned} \frac{d[Auxin]}{dt} &= \frac{k_{1a}}{1 + \frac{[X]}{k_1}} + k_2 + \frac{k_{2a}[ET]}{1 + \frac{[CK]}{k_{2b}}} \frac{[PLSp]}{k_{2c} + [PLSp]} - \\ &\quad (k_3 + k_{3a}[X])[Auxin] + k_{1v auxin}[IAA] \\ \frac{d[X]}{dt} &= k_{16} - k_{16a}[CTR1^*] - k_{17}[X] \\ \frac{d[PLSp]}{dt} &= k_8[PLSm] - k_9[PLSp] \\ \frac{d[Ra]}{dt} &= -k_4[Auxin][Ra] + k_5[Ra^*] \\ \frac{d[Ra^*]}{dt} &= k_4[Auxin][Ra] - k_5[Ra^*] \\ \frac{d[CK]}{dt} &= \frac{k_{18a}}{1 + \frac{[Auxin]}{k_{18}}} - k_{19}[CK] + k_{1vCK}[cytokinin] \\ \frac{d[ET]}{dt} &= k_{12} + k_{12a}[Auxin][CK] - k_{13}[ET] + k_{1veth}[ACC] \\ \frac{d[PLSm]}{dt} &= \frac{k_6[Ra^*]}{1 + \frac{[ET]}{k_{6a}}} - k_7[PLSm] \\ \frac{d[Re]}{dt} &= k_{11}[Re^*][ET] - (k_{10} + k_{10a}[PLSp])[Re] \\ \frac{d[Re^*]}{dt} &= -k_{11}[Re^*][ET] + (k_{10} + k_{10a}[PLSp])[Re] \\ \frac{d[CTR1]}{dt} &= -k_{14}[Re^*][CTR1] + k_{15}[CTR1^*] \\ \frac{d[CTR1^*]}{dt} &= k_{14}[Re^*][CTR1] - k_{15}[CTR1^*] \\ \frac{d[IAA]}{dt} &= 0, \quad \frac{d[cytokinin]}{dt} = 0, \quad \frac{d[ACC]}{dt} = 0 \end{aligned}$$

Table 1 The hormonal crosstalk in Arabidopsis root development model differential equations. See [29] for details.

remove a total of 8 parameters and reduce the dimension of the input space from 31 to 23, by choosing to work with appropriate rate parameter ratios. The specific rate parameter ratios we use as well as the unaltered rate parameters are given in table 2. Also shown are the ranges used to define the initial search space \mathcal{X}_1 , discussed further below.

As we consider ranges of the rate parameters and their ratios which are always positive and span two or more orders of magnitude, we choose to convert to a log scale. Hence we define the 23-dimensional vector x of input parameters for the model as:

$$x = (\log(k_1), \log(k_2/k_{1a}), \dots, \log(k_{1veth}/k_{12})) \quad (21)$$

which corresponds to the first column of table 2, without the inclusion of the control parameter k_6 . It is this vector of inputs x that will be used in the emulator equations (5), (6), (8), (9), and that is directly analogous to the 1-dimensional input x of the simple model given in equations (1) and (2). The Arabidopsis model also requires initial conditions for each of the 15 model outputs [29], and the values used are given in table 3.

Input Rate Parameters	Minimum	Maximum
k_1	0.1	10
k_2/k_{1a}	0.02	2
k_{2a}/k_{1a}	0.28	28
k_{2b}	0.1	10
k_{2c}	1×10^{-6}	1
k_3/k_{1a}	0.2	20
k_{3a}/k_{1a}	0.045	4.5
k_5/k_4	0.1	10
k_6	Control: 0 (<i>pls</i> mutant) or 0.3 (wildtype)	
k_{6a}	0.002	2000
k_7	0.1	10
k_9/k_8	0.1	10
k_{10a}/k_{10}	166	1.66×10^4
k_{11}/k_{10}	166	1.66×10^5
k_{12a}/k_{12}	0.1	10
k_{13}/k_{12}	1	1000
k_{15}/k_{14}	2.83×10^{-4}	0.283
k_{16a}/k_{16}	0.33	33.3
k_{17}/k_{16}	0.033	3.33
k_{18}	0.01	10
k_{19}/k_{18a}	0.01	10
$k_{1v\text{auxin}}/k_{1a}$	0.1	100
$k_{1v\text{CK}}/k_{18a}$	0.1	10
$k_{1v\text{eth}}/k_{12}$	1	100

Table 2 The input or rate parameter ranges that define the initial search region \mathcal{X}_1 over which the history match is performed. Due to symmetries in the model at equilibrium, only ratios of certain parameters will be constrained, hence we choose to work directly with these ratios, as given in the left column. Note that k_6 is a control parameter used to define wildtype or *pls* mutant, and hence is not included in the parameter search.

Model Output	Initial Concentration	Measurement Available
Auxin	0.1	Yes
X	0.1	
PLSp	0.1	
Ra	0	
Ra*	1	
CK	0.1	Yes
ET	0.1	Yes
PLSm	0.1	Yes
Re	0	
Re*	0.3	
CTR1	0	
CTR1*	0.3	
IAA	0 or 1	
cytokinin	0 or 1	
ACC	0 or 1	

Table 3 The list of 15 original model outputs, their initial conditions and whether measurements are available. For simplicity of terminology, exogenous application of IAA, cytokinin or ACC is referred to as "feeding auxin, cytokinin or ethylene". The values of 0 or 1 for IAA, cytokinin and ACC correspond to no feeding or feeding of auxin, cytokinin or ethylene respectively. See [29] for details.

We are primarily interested in the behaviour of the four measurable outputs: [Auxin], [PLSm], ethylene [ET] and cytokinin (represented as [CK] in the model). These were measured for the following cases: wild type (wt), *pls* mutant (mu), wild type fed auxin (fa), wild type fed ethylene (fe), wild type fed cytokinin (fc) and *pls* mutant fed ethylene (mu_fe). The critical behaviour that we want the Arabidopsis model to capture is that of the trends exhibited between certain pairs of measurements. For example, the auxin level is seen to decrease in the *pls* mutant compared to that of the wild type, while it is seen to increase when ethylene is fed to the wild type compared to the wild type with no feeding. A summary of the 16 experimental trends that were used in this analysis is given in table 4 (see [29] for details). The six different experimental scenarios are correspondingly represented in the model by choosing certain values for the control parameter k_6 (which corresponds to the effect of the *PLS* gene) and the initial conditions for IAA, ACC and cytokinin, which represent the concentration of feeding chemicals present. The wild type and *pls* mutant cases correspond to setting $k_6 = 0.3$ and $k_6 = 0$ respectively, while no feeding implies IAA=ACC=cytokinin=0, with IAA=1, ACC=1 or cytokinin=1 corresponding to the feeding of auxin, ethylene or cytokinin respectively (see table 4).

To represent the possible model outputs corresponding to each of the cases, we define the time dependant function h :

$$h_{j,a}(x, t), \quad a \in \{\text{wt, mu, fa, fe, fc, mu_fe}\}$$

$$j \in \{\text{Auxin, PLSm, ET, CK}\}$$

$$x = (\log(k_1), \dots, \log(k_{1v\text{eth}}/k_{12}))$$

where we have introduced a control parameter a that represents the combined choice of plant type and feeding action, the subscript j indexes each of the four measurable chemicals, the vector x represents the vector of rate parameters as before and t represents time.

We are mainly interested in matching the observed trends which are often specified as ratios to wild type. Therefore we choose to work with the log ratio of model outputs, as these will be more robust and allow multiplicative error statements. We also equate these trends to the output of the model at equilibrium [29], that is for $t \rightarrow \infty$, and hence we define the main outputs of interest to be

$$f_i(x) = \lim_{t \rightarrow \infty} \log \left\{ \frac{h_{j,a_2}(x, t)}{h_{j,a_1}(x, t)} \right\} \quad (22)$$

Chemical Output	Trend relative to wild type with no feeding ($k_6 = 0.3$, IAA=ACC=cytokinin=0)				Trend relative to <i>pls</i> mutant with no feeding ($k_6 = 0$, IAA=ACC=cytokinin=0)
	<i>pls</i> mutant ($k_6 = 0$)	Feed Auxin (IAA=1)	Feed Ethylene (ACC=1)	Feed Cytokinin (cytokinin=1)	<i>pls</i> mutant + Feed Ethylene ($k_6 = 0$ and ACC=1)
Auxin	Down	Up	Up	Down	Down
PLSm	-	Up	Down	Down	-
ET	No change	Up	Up	Up	-
CK	Up	Down	Down	Up	-

Table 4 Summaries of the direction of observed trends of the four measurable chemicals, relative to wild type for the four types of experiment: *pls* mutant, feeding auxin, ethylene and cytokinin respectively (first four columns). The final column gives the trend for the case of feeding ethylene to the *pls* mutant, relative to the *pls* mutant with no feeding. See the text and also [29] for more detail on the size and related uncertainties for each of the measured trends.

where the subscript i indexes the elements of the list $\{j, a_1, a_2\}$ corresponding to the 16 trends that were actually measured, as presented in table 4. It is this function $f_i(x)$ that will be directly compared to the observed trends. Again, note the analogy with $f_i(x)$ as defined by equations (1) and (2). We also append to $f_i(x)$ two additional outputs of interest which are not ratios: $\log(h_{auxin,wt}(x, t))$ and $\log(h_{CK,wt}(x, t))$, again evaluated as $t \rightarrow \infty$. These will ensure the acceptable matches found will not have unrealistic concentrations of auxin and cytokinin. Note that the Bayesian emulation and history matching methods we propose could be applied to outputs at any time point, and not just to the equilibrium points of primary interest here.

The primary question that the modeller may ask at this point is whether the outputs of the model, in the form of $f_i(x)$, match the observed trends given in table 4, to within an acceptable level of tolerance, and what is the set \mathcal{X} of all rate or input parameters corresponding to such acceptable matches.

The initial input space \mathcal{X}_1 that we choose to perform the global parameter search or history match over is defined in table 2. This was constructed by specifying ranges on the 23 inputs that covered at least one order of magnitude above and below the single input parameter setting found in [29]. The ranges of some parameters of particular interest were subsequently increased to allow a wider exploration. This means we will explore a biologically plausible space that covers at least two orders of magnitude in every dimension, centred (on a log scale) around the original parameter point. This gives rise to a large space \mathcal{X}_1 , of suitable size to demonstrate our methodology. Note that we could make these ranges wider still if this was deemed plausible, which would simply result in us having to perform more waves to complete the history match.

Linking the Arabidopsis model to reality

The next task is to link the Arabidopsis model formally to reality [6, 7, 15]. The Bayesian paradigm allows us to represent scientific judgements as probabilistic specifications or, if we follow the Bayes Linear approach, as expectation and variance statements [38]. As we do not

have access to the precise quantitative values for the observations z_i that feature in equation 3, we instead propose values for the observations, observation errors $\text{Var}(e_i)$ and model discrepancy $\text{Var}(\epsilon_i)$ that are consistent both with the observed trends given in table 4 and with expert judgement concerning the accuracy of the model and the relevant experiments. We do this for two reasons: firstly to demonstrate that our approach can be reasonably applied to situations where only qualitative data is available, and secondly to highlight what kinds of analysis are possible if quantitative measurements are actually available across all the outputs of interest, hence motivating more detailed future data collection. There are several possible ways to assess these quantities while conserving consistency with the observed trends. We choose a conservative, minimal approach, and specify for the ‘‘Up’’, ‘‘Down’’ and ‘‘No Change’’ trends that $z_i = 1.24, -1.24$ and 0 , and that $\sigma_i = 0.35, 0.35$ and 0.061 respectively, where σ_i represents the combined model discrepancy and observed errors

$$\sigma_i = \sqrt{\text{Var}(\epsilon_i) + \text{Var}(e_i)}. \quad (23)$$

These combined specifications have been made so that the intervals

$$z_i \pm 3\sigma_i \quad (24)$$

represent an increase of between 20% to ten fold for the ‘‘Up’’ trends, a decrease also of between 20% to ten fold for the ‘‘Down’’ trends, and an interval of 40% decrease to 40% increase for the ‘‘No Change’’ trend. These intervals, assumed symmetric on the log scale, were formulated by answering the natural question: where would each model output have to lie to avoid violating the trends given in table 4, considering relevant observational and model uncertainties? This specification captures the main features of the trend data and is sufficient for our purposes of demonstrating the Bayesian history matching methodology. Obviously, a more detailed treatment would involve having more information regarding the observations z_i themselves,

and their associated measurement errors represented by $\text{Var}(e_i)$. Also, were we to consider in more detail the known deficiencies of the model, we could give a more detailed specification of the model discrepancy $\text{Var}(\epsilon_i)$, which would most likely include correlations between different outputs. See [6], [16] and [8] for examples of more detailed model discrepancy specifications in alternative applications, and [18] and [15] for further discussions.

Figure 7 shows all 16 intervals corresponding to the measured trends, as represented by equation (24), given as the black error bars, on a log scale. Also shown (as the first two errors bars from the left) are the two additional non-ratio wildtype outputs for Auxin and Cytokinin, which are given reasonably wide intervals of 0.24 plus or minus an order of magnitude [29].

The specification of z_i , $\text{Var}(e_i)$ and $\text{Var}(\epsilon_i)$ or equivalently σ_i , can be used to define an ‘acceptable match’ between model output and observed data via the implausibility measures of equation (18), as any model evaluation that satisfies $I_i(x) < c$ for some cutoff c . A common choice is $c = 3$, based on Pukelsheim’s 3-sigma rule^[4] (see [43]). We may impose this constraint simultaneously across all of the 18 outputs shown in figure 7, by demanding that $I_M(x) < c$ where $I_M(x)$ is the maximum implausibility defined by equation (19), or we could impose a less stringent criteria by constraining the second or third maximum implausibility instead, which would allow model runs to deviate from one or two outputs respectively.

Bayesian emulation of the Arabidopsis model

We can now proceed with the first wave of emulation of the Arabidopsis model as follows. First we design a set of 2000 wave 1 runs over the initial search region \mathcal{X}_1 based on a maximin latin hypercube design (see figure 3 and [33, 34]), using for example the `lhs()` function in R [36]. Each of these runs specifies a distinct set of values of all the rate parameters in x , and therefore for each run the differential equations given in table 1 were solved numerically using the `lsoda()` function again in R, with initial conditions given in table 3, up to $t = 10000$ seconds to ensure equilibrium is reached (equilibrium was then checked). Each run took approximately 1 second of real time to evaluate, implying that although this is a relatively fast model, it is still too slow to exhaustively search the full 23 dimensional input space, which would likely require a vast number of runs. The emulators that we develop

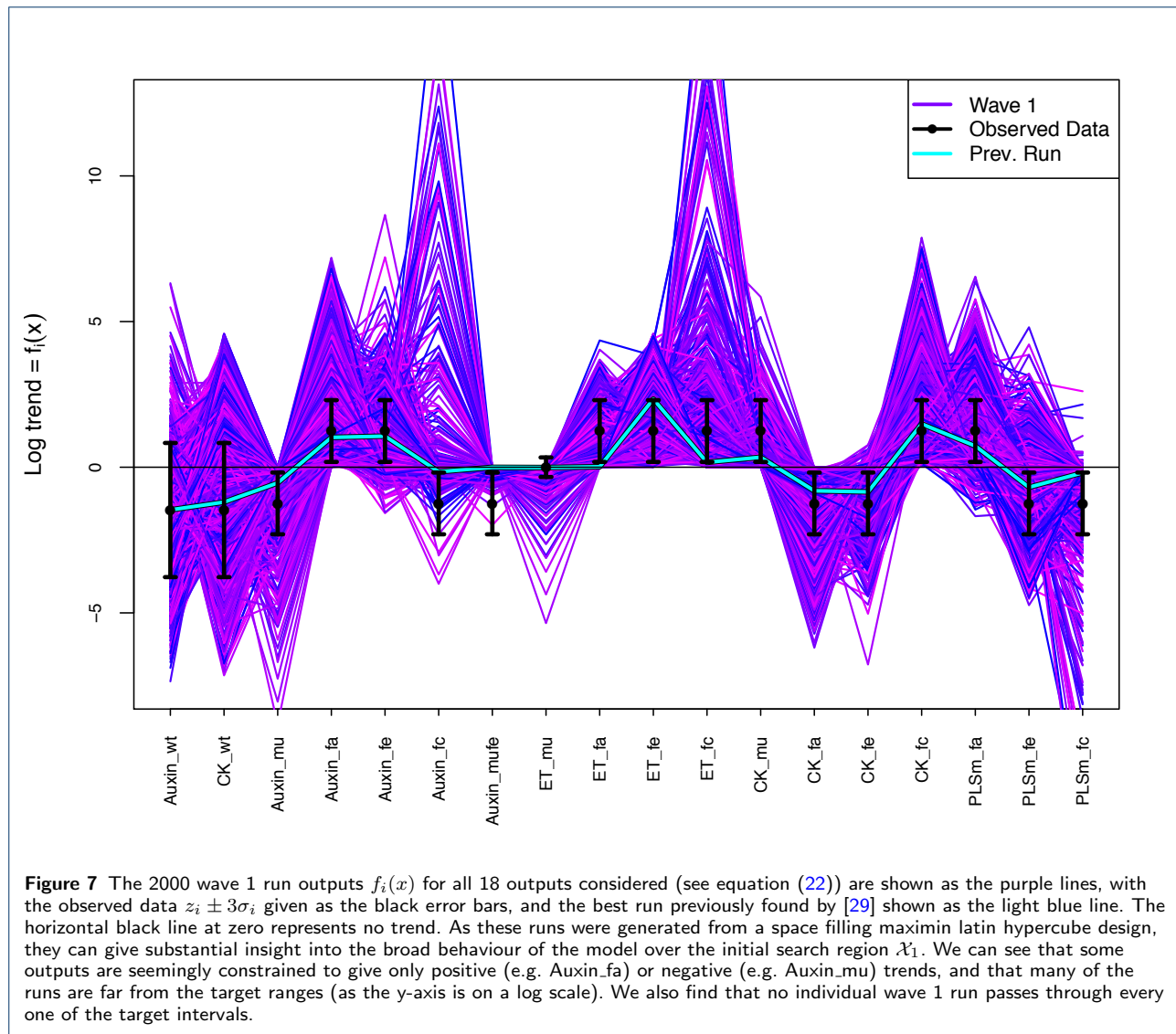
turn out to be 4 orders of magnitude faster than the model, and hence allow a much more detailed and efficient exploration. This ratio of emulator speed versus model speed actually improves as the model complexity increases, as the speed of an emulator is a function of the number of runs used to construct it [6].

The wave 1 run outputs $f_i(x)$ for all 18 outputs considered (see equation (22)) are shown in figure 7 as the purple lines, with the observed data intervals $z_i \pm 3\sigma_i$ given as the black error bars, and the best run previously found by and discussed in [29] shown as the light blue line. As these runs were generated from a space filling design, they can give substantial insight into the broad behaviour of the model over the initial search region \mathcal{X}_1 . We can see that some outputs are seemingly constrained to give only positive (e.g. Auxin_fa) or negative (e.g. Auxin_mu) trends, and that many of the runs are far from the target ranges (as the y-axis is on a \log_e scale). We also find that no individual wave 1 run passes through every one of the target intervals. This all suggests that the volume of the non-implausible space \mathcal{X} containing only acceptable runs may be small or indeed zero, and hence we may need several waves for the history match.

We employ the more general emulator structure as represented by equation (5). For each output $f_i(x)$, we identify the list of active input parameters x_{A_i} by fitting first order polynomials in x and selecting the active inputs based on AIC criteria (using for example the `lm()` and `step()` functions in R [36]). We choose the set of deterministic functions $g_{ij}(x_{A_i})$ by selecting terms from the complete third order polynomials in the active inputs, discarding terms again based on AIC criteria (see [6, 7, 15, 22] for more details). Due to the large number of runs and in the absence of strong prior information, we set $E(\beta_{ij}) = 0$ and take a large $\text{Var}(\beta_{ij})$ limit. The β_{ij} terms will hence behave, after the Bayes Linear update represented by equations (8) and (9), approximately like their Ordinary Least Squares linear model fits (see [6] for details).

We choose the combination of the Gaussian process and nugget variances $\sigma_{c_i}^2 = \sigma_{u_i}^2 + \sigma_{w_i}^2$ to be equal to the residual standard error from the OLS linear model fit [6], and set $\sigma_{w_i}^2 = p\sigma_{c_i}^2$ where p is a parameter governing the proportion of variance explained by the inactive variables, taken to be between 0.05 to 0.1, and checked with emulator diagnostics described below. Note that we could design more runs that vary the inactive variables to assess p more accurately, as is done in [6]. Following the arguments presented in [6] for choosing correlation lengths for emulators that contain low order polynomials, we set the (scaled) correlation lengths θ_i , required for equation (6), to be 0.35, where the inputs x have all been scaled to the range $[-1, 1]$.

^[4]Pukelsheim’s 3-sigma rule is the powerful result that states that any continuous unimodal distribution will have a least 95% of its probability within $\mu \pm 3\sigma$, regardless of any asymmetries, large skew or heavy tails.



Finally, we constructed the emulators by using the Bayes Linear update equations (8) and (9) to obtain $E_{D_i}(f_i(x))$ and $\text{Var}_{D_i}(f_i(x))$ for each output i , where D_i is the corresponding vector of 2000 run output values. Emulator diagnostics were then performed by evaluating 200 new diagnostic runs and comparing them to the corresponding emulator predictions, in the form of prediction intervals $E_{D_i}(f_i(x)) \pm 3\sqrt{\text{Var}_{D_i}(f_i(x))}$ (see [39] for detailed emulator diagnostics). In the first wave we found that 13 out of the 18 outputs were straightforward to emulate, in that their emulators were of sufficient accuracy to allow reasonably large parts of the input space to be removed, while simultaneously satisfying emulator diagnostics. The remaining 5 outputs were left to be considered in later waves. Each of these 13 outputs (that define Q_1) required between 7-13 active inputs x_{A_i} , out of

a total of 31 full or 23 reduced input parameters x , which represents a substantial dimensional reduction and hence a large benefit to the emulator construction process and subsequent parameter search, as discussed in [15]. This is in addition to the speed increase of using emulators as they are in this case 10^4 times faster to evaluate than the full Arabidopsis model. Note that each one of the 23 inputs featured in at least one of the 13 emulators.

History matching the Arabidopsis model

We now employ the iterative history matching strategy described above to the Arabidopsis model.

As well as the maximised implausibility $I_M(x)$ defined by equation (19), we also use the more robust second and third maximum implausibilities denoted $I_{2M}(x)$ and $I_{3M}(x)$ respectively, defined using the set

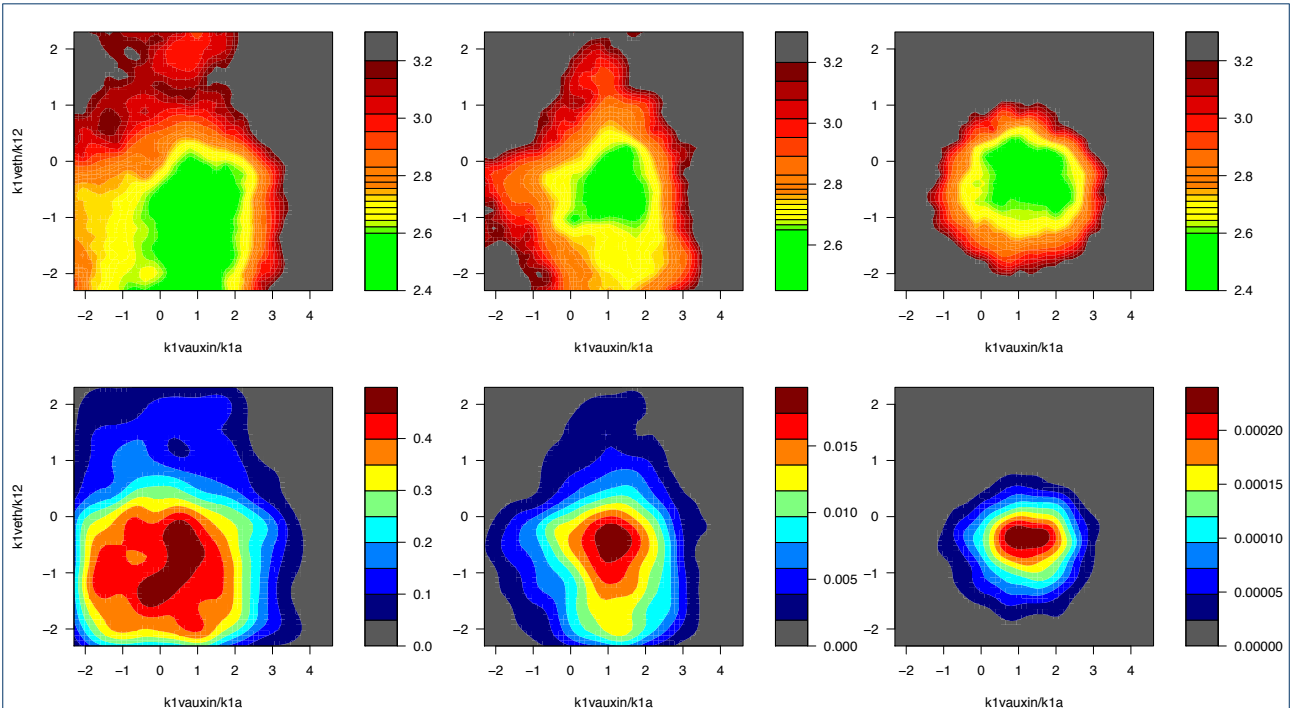


Figure 8 Two different ways to view the non-implausible input or rate parameter space (on a log scale) after waves 1, 2 and 4 (left, middle and right columns respectively). The top row gives the minimised implausibility $I_P(x')$, where $x' = (k_{1vauxin}/k_{1a}, k_{1veth}/k_{12})$. The red and dark grey regions imply that no matter what values are chosen for the remaining 21 inputs, the model will still be a poor match to the data for these settings of $k_{1vauxin}/k_{1a}$ and k_{1veth}/k_{12} . The bottom row gives the optical depth $\rho(x')$ which shows the thickness or depth of the non-implausible region \mathcal{X}_k in the remaining 21 input dimensions, as a proportion of the depth of the original space \mathcal{X}_1 .

Q_k of outputs considered in wave k , as these implausibility measures are more robust to emulator failure. In the first wave, only $I_{2M}(x)$ and $I_{3M}(x)$ were used with conservative cutoffs c of 3.25 and 3 imposed respectively. This defined \mathcal{X}_2 : the non-implausible space remaining after wave 1, which had a volume of 2.06×10^{-1} of the original input space \mathcal{X}_1 .

Figure 8 top left and bottom left panels show two ways of visualising the shape of the non-implausible region \mathcal{X}_2 resulting from the wave 1 analysis. The former is the minimised implausibility plot. This is formed by using the emulators to evaluate the implausibility of a large number of points within the 23 dimensional \mathcal{X}_1 . These implausibilities are then projected down to two dimensions (the input parameters $k_{1vauxin}/k_{1a}$ and k_{1veth}/k_{12} in this case) by minimising the implausibility over the remaining 21 dimensions. If we partition x into (x', x'') where x' is the two dimensional vector representing the inputs we wish to project onto and x'' is the remaining 21 inputs, then the minimised implausibility is defined as:

$$I_P(x') = \min_{x''} I_M(x', x'') \quad (25)$$

The plot has the following interpretation: the red/dark grey regions correspond to high implausibility and imply that no matter what values we choose for the remaining 21 inputs, the Arabidopsis model will not give good matches to the data in these regions of $(k_{1vauxin}/k_{1a}, k_{1veth}/k_{12})$ space. The green/yellow regions imply that somewhere within the 21-dimensional space there are low implausibility points with these values of $k_{1vauxin}/k_{1a}$ and k_{1veth}/k_{12} . We are therefore looking at the silhouette of \mathcal{X}_2 for various different cutoffs represented as colours [7]. The green and yellow regions will be investigated further in subsequent waves.

The bottom left panel of figure 8 shows an optical depth plot again for the inputs $k_{1vauxin}/k_{1a}$ and k_{1veth}/k_{12} . This gives the 21 dimensional thickness or depth of \mathcal{X}_2 as a proportion of total depth, for each point x' in the 2-dimensional $(k_{1vauxin}/k_{1a}, k_{1veth}/k_{12})$ space. It is defined as

$$\rho(x') = \frac{V_{21}\{x \in \mathcal{X}_2 \mid x' \text{ fixed}\}}{V_{21}\{x \in \mathcal{X}_1 \mid x' \text{ fixed}\}}, \quad (26)$$

Wave	Outputs Emul.	Active Inputs	Cutoffs c used			Prop. Space Non-imp.
			I_M	I_{2M}	I_{3M}	
1	13	7-13	-	3.25	3	2.06×10^{-1}
2	18	6-15	-	3.1	2.8	4.83×10^{-3}
3	18	6-16	5	2.9	2.7	4.34×10^{-4}
4	18	11-19	3.2	2.8	2.65	2.69×10^{-5}
5	-	-	3.2	-	-	1.21×10^{-6}

Table 5 Summary of the 4 waves of emulation. Col. 2: no. of outputs emulated, Col. 3: the no. of active inputs used; Col. 4-6: the implausibility thresholds; Col. 7: the proportion of the parameter space deemed non-implausible. The 5th wave was performed but not emulated.

where $V_{21}\{\cdot\}$ denotes the 21-dimensional volume of the remaining space. $\rho(x')$ can therefore show where large or small amounts of non-implausible points can be found, conditioned on x' , providing further insight into the structure of \mathcal{X}_2 . Both $I_P(x')$ and $\rho(x')$ are generalisable to higher dimensions if necessary, and various computational shortcuts in the emulator calculations can be exploited (see [6, 7, 15, 22] for details).

We then proceeded with a total of 4 waves of emulation and history matching. Summaries of the waves' properties in terms of outputs emulated, numbers of active inputs used, and cutoffs and implausibility measures employed can be found in table 5. The final column gives the proportion of non-implausible space remaining in terms of the original input space, after each wave. At each wave emulator diagnostics are performed by evaluating another 200 model runs over the current non-implausible space, and checking that the new emulators predict these 200 runs with appropriate accuracy (see [39] for more details on emulator diagnostics).

Figure 8 middle and right columns, show the minimised implausibility and optical depth plots after wave 2 and wave 4 respectively, again for the inputs $k_{1vauxin}/k_{1a}$ and k_{1veth}/k_{12} , and highlight the progression of the history match and the sequential reduction of the non-implausible space. Note that in the optical depth plot after wave 4 (bottom right panel), the depth of the non-implausible region is now very small. Even if we were to set the inputs $k_{1vauxin}/k_{1a}$ and k_{1veth}/k_{12} to values corresponding to the largest depth (given by the dark red region), the chances of finding a non-implausible point by randomly choosing the other inputs is approximately 2.3×10^{-4} , highlighting the difficulty of manual or ad hoc searches of the input space.

The history matching process is terminated with the evaluation of a wave 5 set of uniformly drawn acceptable runs. As shown in table 5, the non-implausible space \mathcal{X} was now 1.21×10^{-6} smaller than that of the original \mathcal{X}_1 : a small target, which would require on average a total of 830000 runs chosen at random to obtain 1 single acceptable run, requiring approximately

230 hours of processor time. In contrast, our history matching approach generated hundreds of acceptable runs using only 10000 model evaluations, requiring approximately 2.7 hours of processor time. For a more expensive model in terms of evaluation time, such efficiency gains would be even more dramatic [6, 7, 15].

We now go on to describe the results of the parameter search and discuss their implications.

Discussion of the results of the parameter search

Figure 9 shows the wave 5 minimised implausibility (below diagonal) and optical depth (above diagonal) plots for the 12 most informed input rate parameters, as labelled along the diagonal. For example, the top right panel gives the optical depth plot with k_{1veth}/k_{12} on the x-axis and k_{2a}/k_{1a} on the y-axis, while the bottom left plot gives the corresponding minimised implausibility plot with the x- and y-axis swapped. The input location in parameter space of the previous best run as described in [29] is shown as the single white point in all panels: this corresponds to the single light blue run in figure 7. Along the main diagonal, 1-dimensional optical depth plots are given, showing that we have learnt most about inputs k_{16a}/k_{16} , k_{18} , k_{19}/k_{18a} , $k_{1vauxin}/k_{1a}$ and k_{1veth}/k_{12} . All inputs that are not shown in this plot were either not constrained at all, or only loosely constrained by the observed data. Often, a ‘‘pairs plot’’ such as shown in figure 9, can provide much insight into both the structure of the model and the complex constraints placed upon the input rate parameters by the data. For example, we instantly see that input k_{16a}/k_{16} is highly constrained and must lie close to a value of 1/0.3, which we can see is the value that precisely balances the first two terms on the right hand side of the differential equation for dX/dt (given in table 1), when $CTR1^*$ obtains its maximum value of 0.3. The k_{13}/k_{12} vs k_{2a}/k_{1a} panel (top row, fifth along from the left) shows a linear relationship (on a log scale) between k_{13}/k_{12} and k_{2a}/k_{1a} , in that high values of k_{13}/k_{12} require high values of k_{2a}/k_{1a} to compensate them, and vice versa. The input k_{6a} , for which a large range was explored, is constrained to lower values, and has subtle relationships with both the inputs k_{2a}/k_{1a} and k_{2c} (see the panels third from the left in the top two rows). This has important consequences as discussed below. We also see that although the previous best run is close to being an acceptable input point, it is not actually contained within the wave 5 non-implausible volume, as can be seen from the k_{11}/k_{10} vs k_{15}/k_{14} plot. This implies that we now have a large number of wave 5 runs that are superior fits to the data than were previously found.

Figure 10 shows the waves 1, 3 and 5 runs as the purple, green and red lines respectively, for the 18 model

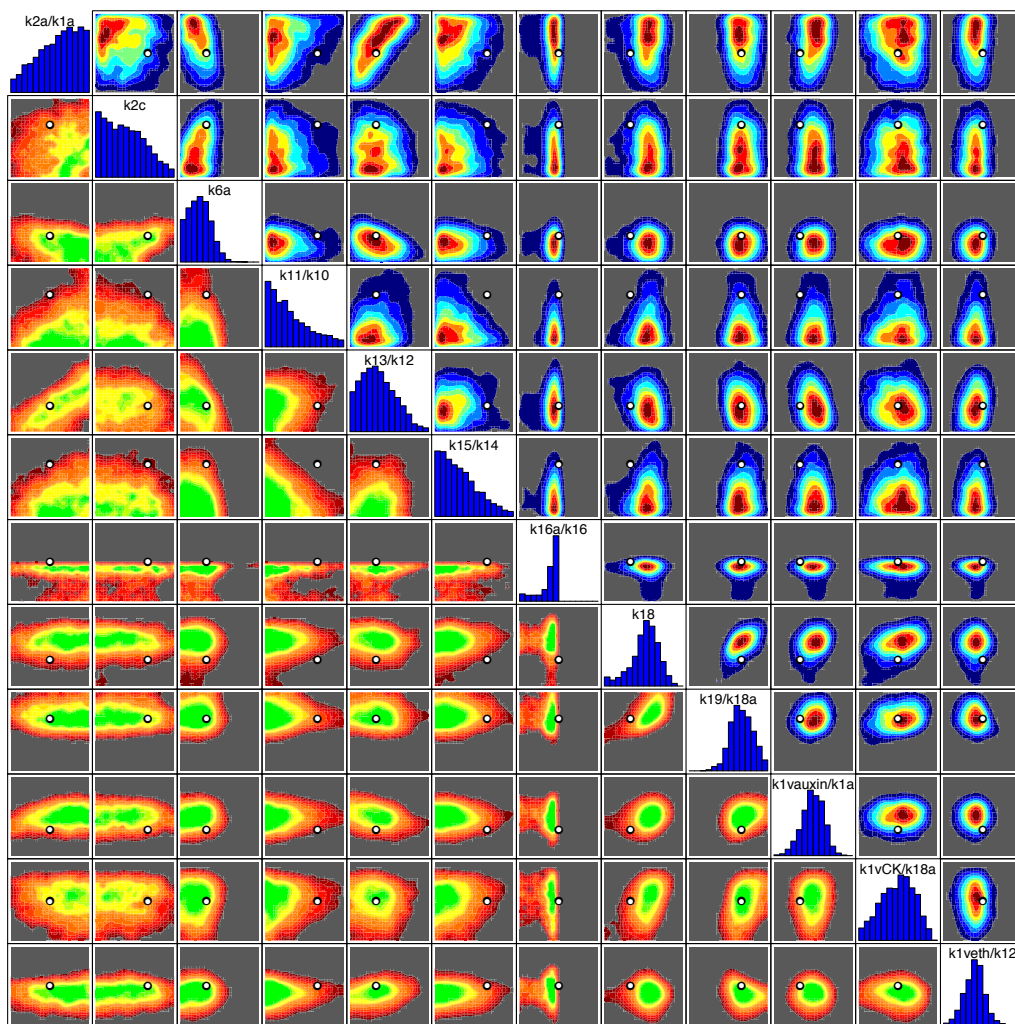
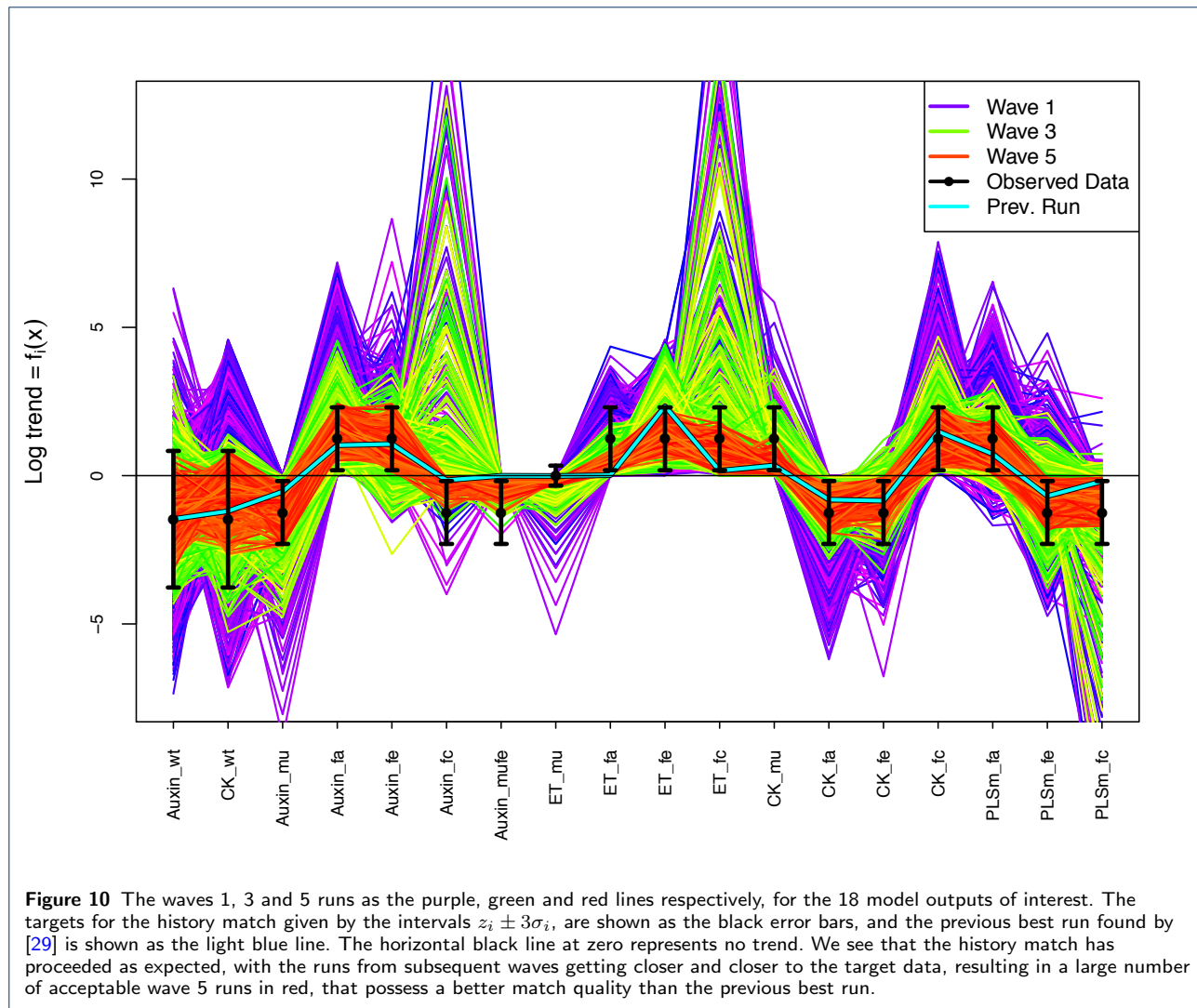


Figure 9 The wave 5 minimised implausibility (below diagonal) and optical depth (above diagonal) plots for the 12 most informed input rate parameters, as labelled along the diagonal. Note that the input rate parameters are on a log scale as given by equation (21) with ranges consistent with table 2. The input location of the previous best run as described in [29] is shown as the single white point. Along the main diagonal, 1-dimensional optical depth plots are given.

outputs of interest. The targets for the history match given by the intervals $z_i \pm 3\sigma_i$, are shown as the black error bars, and the previous best run found by [29] is again shown as the light blue line. Note that the first two error bars correspond to the extra two outputs of Auxin and CK wildtype with no feeding, while the remaining 16 are the trend data from table 4. The horizontal black line at zero represents no trend. We see that the history match has proceeded as expected, with the runs from subsequent waves getting closer and closer to the target data. In wave 1, none of the runs simultaneously passed through all the targets, which we now know is due to \mathcal{X} being so small (1.21×10^{-6}), however we now have hundreds of acceptable runs from within \mathcal{X} shown here as the wave 5 red runs, all of

which are a better match than the previous best run, and we can quickly generate more.

Figure 10 also informs as to the class of possible observed data sets that the model could have matched, and hence gives insight into the model's flexibility. We see that 6 out of the 16 trend outputs could have predicted either positive or negative (or zero) trends, and hence could possibly have fitted many different data sets, although further investigation of the joint structure of these outputs would be required to confirm this. For example, if these 6 outputs were found to vary independently, then they could be adjusted to fit *any* combination of positive, negative (or zero) trends. However the remaining 10 trend outputs are restricted to giving the 'correct' trend, and hence seem not to be flexible at all. In general, we may be concerned about



an overly flexible model, possessing say a high number of rate parameters, and specifically about claims that it has been validated based purely on a comparison to data, as it would be no surprise when it fits the observed data well, and therefore it may not contain much inherent biological structure at all. This is clearly not the case for the Arabidopsis model considered here. Only by performing a global parameter search such as described here, can one guard against such issues.

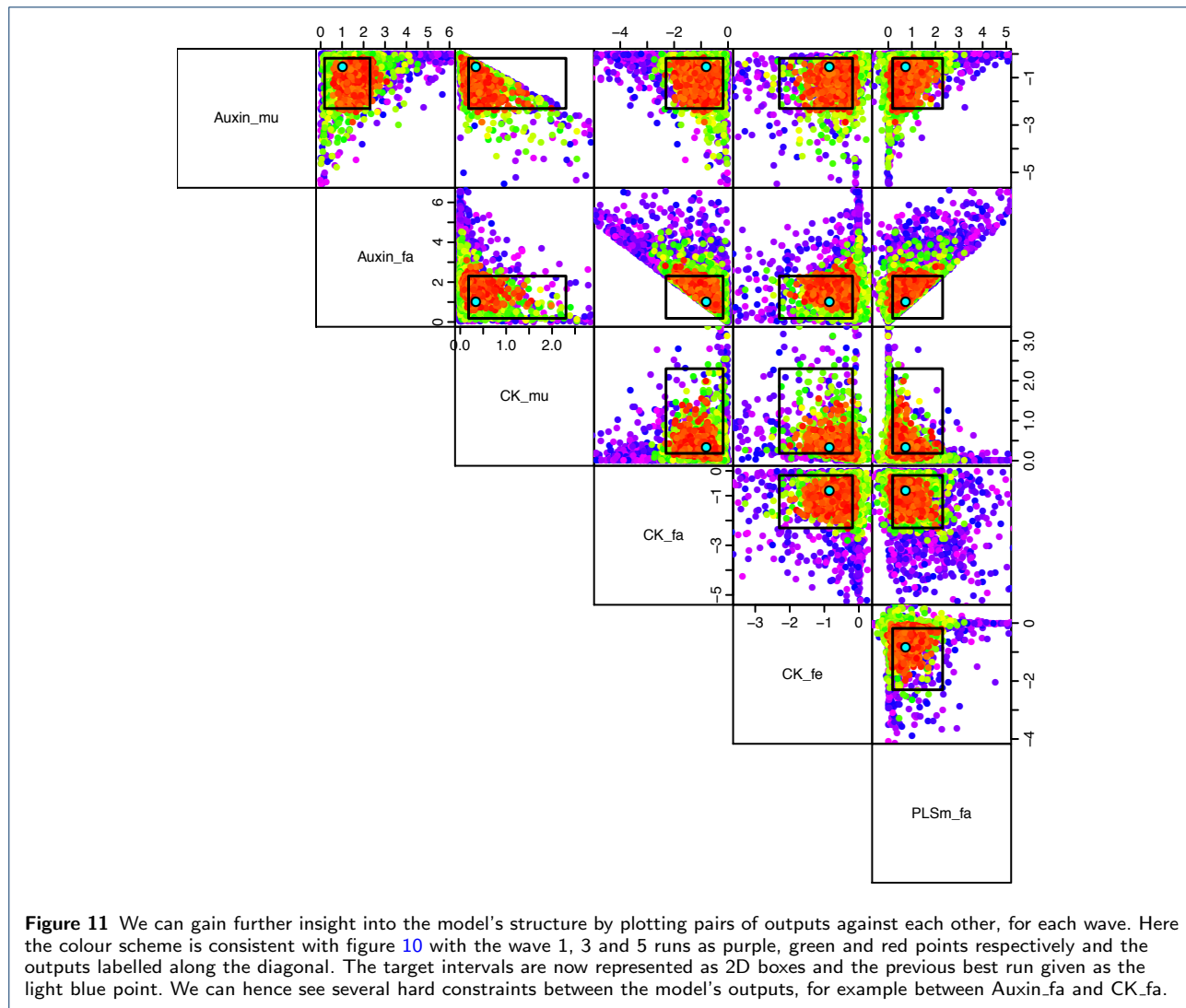
We can gain further insight into the model's structure by plotting pairs of outputs against each other, for each wave, as is shown in figure 11. Here the colour scheme is consistent with figure 10 with the wave 1, 3 and 5 runs as purple, green and red points respectively, the target intervals are now represented as 2D boxes and the previous best run given as the light blue point. The top right panel, for example, shows the Auxin output for the *pls* mutant strain (Auxin_mu)

on the y-axis and the PLSm output with Auxin feeding (PLSm_fa) on the x-axis. This suggests that large negative trends for the Auxin_mu output can only occur when the PLSm_fa trend is close to zero. Similarly, a high PLSm_fa trend implies Auxin_mu must also be close to zero. These plots also highlight previously unknown model constraints between the outputs e.g. the Auxin_fa vs CK_fa panel shows that these two trends satisfy a strict inequality in log space that bisects the target box. Similar strict constraints are seen in the Auxin_mu vs CK_mu and Auxin_fa vs PLSm_fa panels. We now go onto discuss in more detail the implications for gene functions of the parameter search results.

Discussion

Evaluation of gene functions using Bayesian emulation methodology

In the previous sections, we have shown that Bayesian emulation and history matching methodology allows



extensive exploration of the input rate parameter space, giving multiple insights into the model's structure, constraints placed upon it by the observed data and on the corresponding biological consequences.

Here we further demonstrate that this methodology can be used to evaluate regulatory relationships and gene functions in hormonal signalling systems, by examining both the above results and the results obtained from a second history match of an alternative model.

The k_{6a} rate parameter describes the regulatory strength of ethylene as applied to the PLS transcriptional rate. It features in the first term on the right hand side of the $d[PLSm]/dt$ equation in table 1, and in the limit $k_{6a} \rightarrow \infty$ we have that

$$\frac{k_6[Ra^*]}{1 + \frac{[ET]}{k_{6a}}} \longrightarrow k_6[Ra^*] \quad (27)$$

Therefore increasing k_{6a} decreases this regulatory strength. Thus, low values of k_{6a} indicate that a regulatory relationship of ethylene inhibiting PLSm production is required. The optimal depth and minimised implausibility plots corresponding to k_{6a} in Figure 9 show that high values of k_{6a} are ruled out. Our analysis suggests that no acceptable parameter combinations with large k_{6a} can be found that are consistent with the target data, and hence our results strongly support the assertion that the inhibition of PLSm production by ethylene is required for predicting known experimental trends, conditional on the remaining specifications made in the analysis.

The k2c parameter describes the very important question of whether the PLS gene has a function in auxin biosynthesis. Examining the third term on the right hand side of the $d[Auxin]/dt$ equation in table 1,

we see that as $k_{2c} \rightarrow 0$ we have that

$$\frac{k_{2a}[ET]}{1 + \frac{[CK]}{k_{2b}}} \frac{[PLSp]}{k_{2c} + [PLSp]} \rightarrow \frac{k_{2a}[ET]}{1 + \frac{[CK]}{k_{2b}}} \quad (28)$$

Therefore the $k_{2c} = 0$ case implies that the *PLS* gene has no direct function in auxin biosynthesis, where the $k_{2c} > 0$ case would imply that it does. However, for several of the outputs considered, $[PLSp]$ can also tend to zero, implying that the limit given in equation (28) is not uniquely defined, and that the original model is not continuous at $k_{2c} = 0$. Hence, to answer questions regarding the role of the *PLS* gene in auxin biosynthesis we cannot simply examine low values of k_{2c} . As the $k_{2c} = 0$ case effectively defines a distinct model, we perform a new 5 wave history match to find any acceptable matches to the observed data, following the same methodology as described above. The results of the new history match are given in figure 12, and notably we again found several acceptable wave 5 runs shown as the red lines, that are in agreement with the observed trends. The acceptable runs were found in a smaller region than previously, with a volume of \mathcal{X} approximately 2.4×10^{-8} of that of \mathcal{X}_1 .

Comparing the results of the $k_{2c} = 0$ case (figure 12) with the results of the $k_{2c} > 0$ case (figure 10) we can immediately see some important differences between the two models. For the Auxin_mufe output (7th error bar from the left), the $k_{2c} > 0$ model always returns the correct negative trend. In contrast the $k_{2c} = 0$ model returned the incorrect positive trend for the vast majority of the wave 1, 2 and 3 runs, implying that there is only a very small region of input space that returns the correct negative trend, a region located by the history match analysis and explored by the wave 5 runs. Without such an analysis it would be easy to incorrectly conclude that the $k_{2c} = 0$ model is inconsistent with the observed data. This demonstrates perhaps the **most important difficulty** in exploring high dimensional models: there may be one (or more) extremely small regions of input space of scientific interest, and conventional optimisation techniques may easily get stuck in local minima far away from these regions. Our Bayesian history matching approach however is specifically designed to combat such difficulties by carefully exploring the space using efficient emulator based global search methods, as we have demonstrated here.

After considering that the *PLS* gene is required for the response of ethylene downstream based on experimental observations (mathematically this is equivalent to the response of ethylene downstream, X , remaining constant for the *pls* mutant ($k_6=0$) fed with ethylene), previous research [29] deduced that the *PLS*

gene does indeed have a function in auxin biosynthesis. However, the history match of the $k_{2c} = 0$ model (figure 12) suggests that, given the specification of the trends and their relevant uncertainties, the $k_{2c} = 0$ model is consistent with observed data, and hence it may not be essential for the *PLS* gene to play a role in auxin biosynthesis.

However, examining the differences between the two models reveals some interesting results. Figure 13 summarises the history match results of both the $k_{2c} > 0$ and $k_{2c} = 0$ models. It shows a comparison of the spread of input parameter locations of the acceptable runs found for the $k_{2c} > 0$ model (red box plots) and the $k_{2c} = 0$ model (blue box plots) in terms of individual input rate parameters as labelled along the x-axis. Note that the two sets of acceptable runs being compared correspond to the red lines in figures 10 and 12 respectively. The y-axis is on a \log_{10} scale, and the grey rectangles show the initial ranges that define the original search region \mathcal{X}_1 as given in table 2. The light blue horizontal lines show the input parameter values of the previous best run as found by [29]. The main differences between the two models' acceptable runs are exhibited by the following parameters or ratios of parameters: k_2/k_{1a} , k_{2b} , k_3/k_{1a} , k_{3a}/k_{1a} , k_{12a}/k_{12} , k_{15}/k_{14} , k_{18} , k_{19}/k_{18} . To the best of our knowledge, the biological significance of many of these differences cannot be judged using current biological insight. However, two ratios, k_2/k_{1a} and k_{3a}/k_{1a} , do reveal some important results. k_{1a} is the maximal rate of transporting auxin from shoot to root; k_2 is the background auxin biosynthesis rate; k_{3a} is the rate constant describing the control of ethylene downstream over auxin transport from root to shoot. First, biologically k_2/k_{1a} must be very small. This is because the background auxin biosynthesis rate, k_2 , must be very small and usually biologically negligible, as it represents the non-enzymatic process in auxin biosynthesis. Moreover, auxin transport from shoot to root, whose maximal rate is k_{1a} , is an important process, as evidenced experimentally [45]. Therefore, k_{1a} should be large. However, for the $k_{2c} = 0$ model to match target data, the majority of acceptable runs have relatively large k_2/k_{1a} , while for the $k_{2c} > 0$ model much smaller and more realistic values are preferred. Second, biologically k_{3a}/k_{1a} should be small. This is because it is known that auxin more predominantly transports from shoot to root, to form an auxin concentration maximum in the root tip [46, 47]. However, for the $k_{2c} = 0$ model to match target data, the set of acceptable runs suggest that relatively large k_{3a}/k_{1a} is required. Therefore, the differences between the two models' parameter ratios highlight that, although we have found acceptable matches for the $k_{2c} = 0$ model, these matches

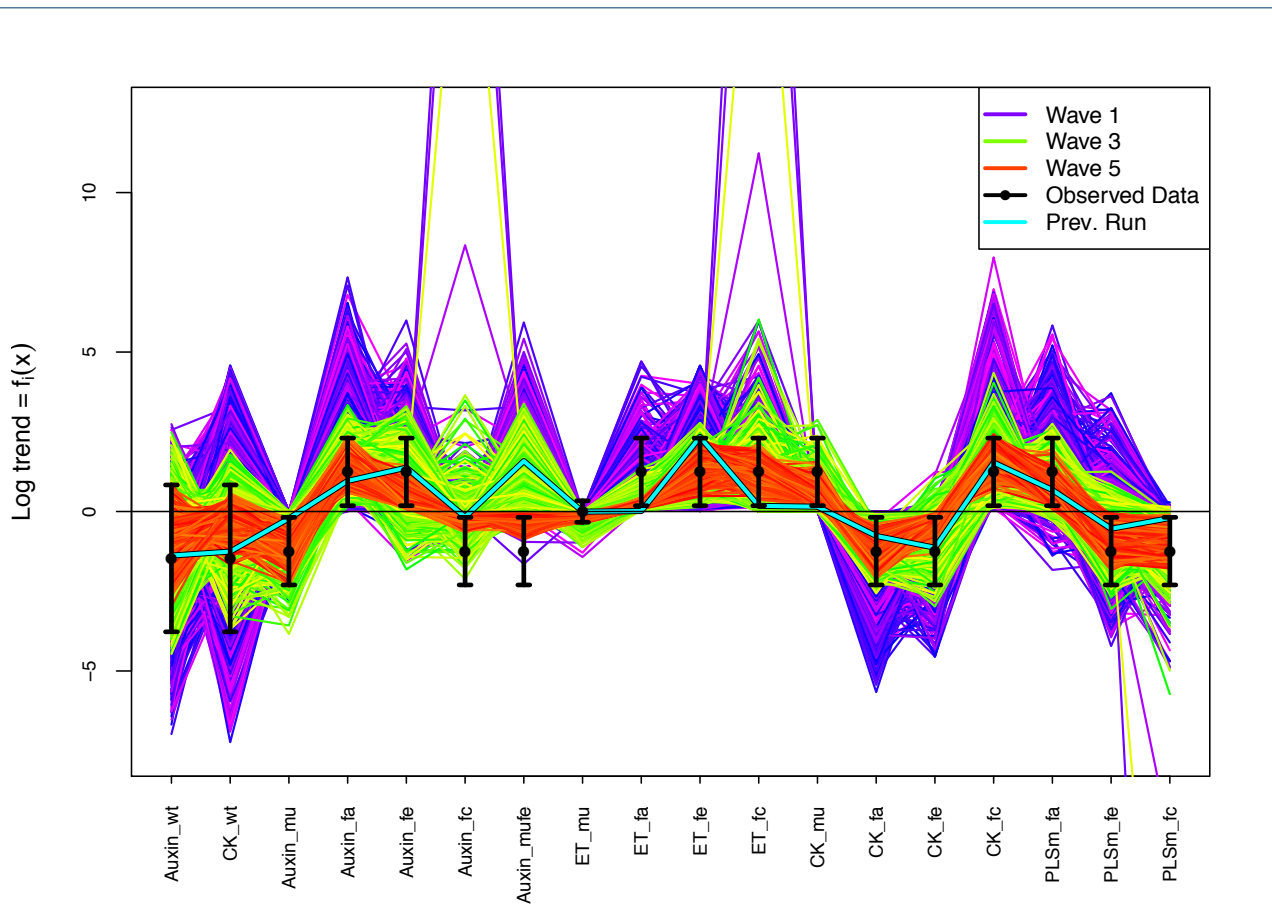
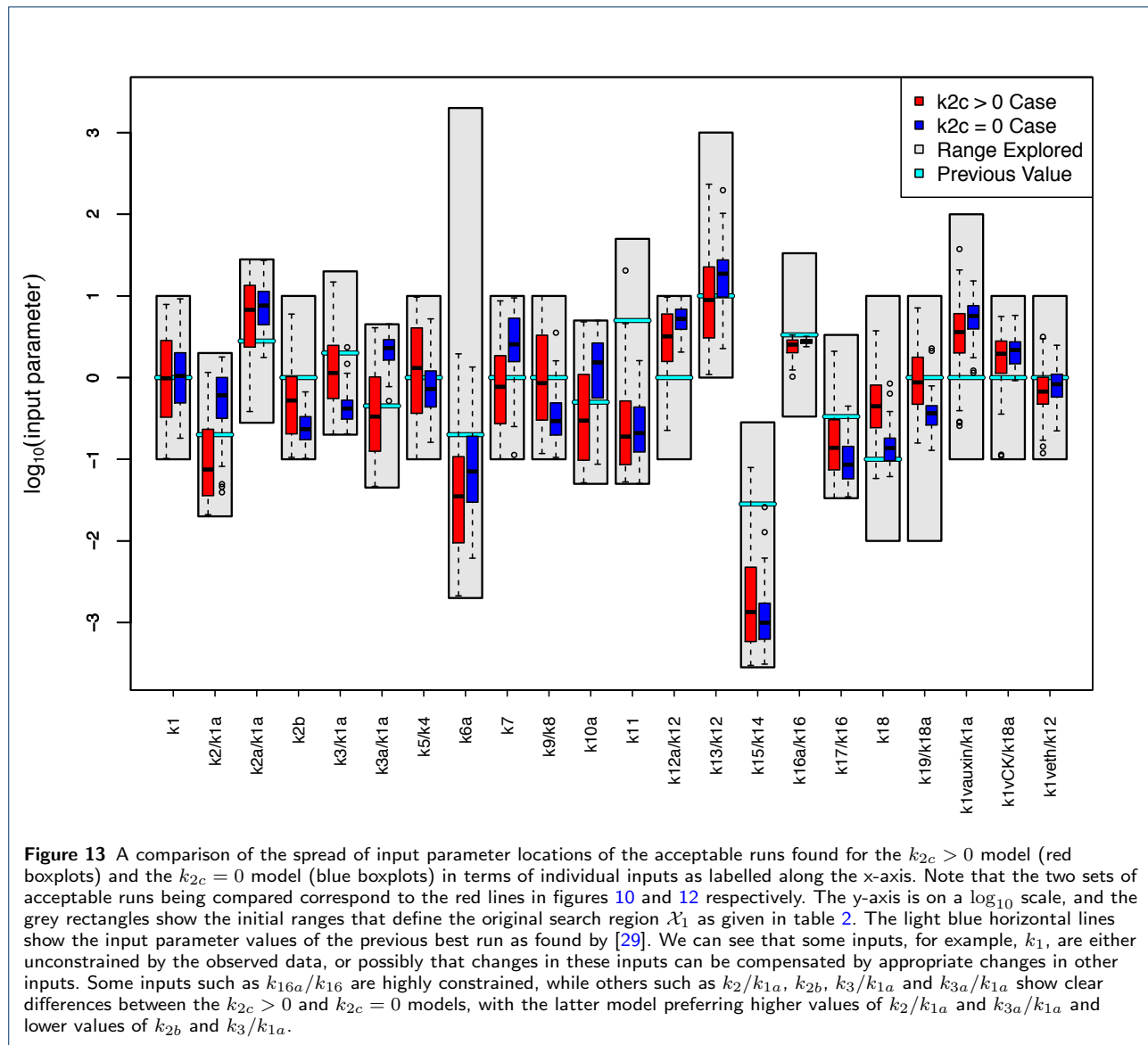


Figure 12 The results from the history match of the $k_{2c} = 0$ model, showing the waves 1, 3 and 5 runs as the purple, green and red lines respectively, for the 18 model outputs of interest. We see that a large number of acceptable wave 5 runs have been found that match the target data (the black error bars) and hence that the reduced $k_{2c} = 0$ model is still consistent with the specified observational data, within a small region of the input space. Comparison with figure 10 shows the main differences between the two models, most noticeably in the Auxin_muFe output (7th error bar from the left) for which the vast majority of the input space returns an incorrect positive trend for the $k_{2c} = 0$ model, as can be seen by the large number of wave 1 and 3 lines above zero, with only a small and hence hard to find region returning the correct negative trend. The $k_{2c} > 0$ model conversely, always returns the correct negative trend.

have not been found at biologically realistic parameter values. While we must be cautious about such conclusions that are based on the finite sampling of the non-implausible regions, we have generated hundreds of approximately uniformly sampled acceptable runs from each model that do indeed exhibit the features discussed. Therefore our results suggest that biological insight clearly favours the model with $k_{2c} > 0$, i.e. that the *PLS* gene does have a function in auxin biosynthesis. More detailed measurements of the key outputs that restrict k_2/k_{1a} and k_{3a}/k_{1a} would of course further clarify this issue.

Our results show that Bayesian emulation and history matching methodology can be used to evaluate regulatory relationships and gene functions in hormonal signalling systems. To further improve the ac-

curacy of the results of this methodology, the following aspects should be considered. First, experimental data should be more quantitatively measured, to define more accurate trends. The example trends we have used in this work, as summarised in table 4 and the associated discussion, are mainly formulated based on qualitative or semi-quantitative experimental data, combined with scientific judgement. Second, model development should include more components, to better describe the experimental systems. Third, Bayesian emulation methodology should be used to study the effects of additional experiments, such as the response of ethylene downstream when feeding ethylene, *etr1* mutant and *etr1-pls* double mutant, on the evaluation of regulatory relationships and gene functions. Fourth, Bayesian emulation methodology should also be used



to explore the effects of the uncertainty of quantitative trends on the evaluation of regulatory relationships and gene functions, as in most cases trends of biological data are not sufficiently quantitative.

Conclusions

We have provided an introduction to the study of complex systems biology models using Bayes linear uncertainty analysis. This represents a possible solution to the fundamental challenge that faces systems biology in terms of the necessity of global parameter searches of high dimensional models. Our approach features three main aspects:

- A more formal statistical model linking the biological model to reality, which encompasses major

sources of uncertainty such as observational errors and model discrepancy.

- A Bayesian emulator allowing a very fast exploration of model behaviour, applicable to models even with very long evaluation times.
- A careful history match using implausibility measures that performs an iterative global exploration of the input parameter space using the emulators, to find the region containing *all* acceptable matches to the observed data.

We applied this methodology to two versions of the hormonal crosstalk in Arabidopsis root development model, and in each case identified the small region of input space containing scientifically interesting matches. The two models and their biological implications were then compared in a robust manner and

used to discuss gene functions. We found that although some acceptable matches to the specified trends could be found for the $k_{2c} = 0$ model, these were only found at parameter settings that violated other known biological evidence, whereas the $k_{2c} > 0$ model's acceptable matches seemed far more realistic. This implied that PLS does indeed play a role in auxin biosynthesis. Our results also strongly supported the assertion that the inhibition of PLSm production by ethylene is required for consistency with known experimental trends.

We would stress that searching for all acceptable matches between model output and observed data is vital for several reasons. It avoids the danger of false conclusions being made, based on the analysis of a single run (or a small number of runs) consistent with the data: conclusions that could easily change if an alternative run was found instead, that also matched the data but which provided different biological implications. If we want to use the model to make predictions for the results of future biological experiments, all acceptable matches must be found and the corresponding range of predictions examined. A narrow range of predictions from the acceptable runs for a particular proposed future experiment, for example, would imply that it would be a good test of the model as it could possibly rule it out, while a large range implies that this experiment would most likely be informative for the model's rate parameters. Model predictions, using all the acceptable runs, can then be used to design efficient sets of future experiments that are most likely to realise particular scientific goals, such as learning about all or subsets of the rate parameters, testing the model or distinguishing between certain biological hypotheses. We would assert that this design problem is also a fundamental challenge to the area of systems biology, but leave a detailed exposition to future work [41, 42].

Since plant root development is regulated by multiple hormones in a coordinated way [48], unravelling the regulatory relationships and gene functions for root development is a difficult task that requires the investigation of how biological information is spatiotemporally integrated and communicated [49]. Modelling hormonal crosstalk as an integrative system is an important aspect for integrating information in plant root development [5, 29, 50–53]. This work demonstrates that a combination of experimental data, a model of hormonal crosstalk in *Arabidopsis* root development, and Bayesian emulation and history matching methodology is able to evaluate regulatory relationships and gene functions in a hormonal signalling system. In particular, Bayesian emulation and history matching methodology is an essential method for performing a global parameter search to attempt to find

all input parameter settings that achieve an acceptable match.

Competing interests

The authors declare that they have no competing interests.

Author's contributions

IV, JL, MG and KL conceived the idea. IV and JL designed this research and carried out the data analysis. IV and MG developed and performed the Bayesian emulation uncertainty analysis. All authors established the links between the Bayesian emulation methodology and hormonal crosstalk in plant development. IV, JL, MG and KL wrote the manuscript.

Acknowledgements

JL and KL gratefully acknowledge the Biotechnology & Biological Sciences Research Council (BBSRC) for funding in support of this study. JR is in receipt of a BBSRC studentship. IV and MG gratefully acknowledge MRC and EPSRC funding.

Author details

¹Department of Mathematical Sciences, Durham University, South Road, DH1 3LE, Durham, UK. ²School of Biological and Biomedical Sciences, Durham University, South Road, DH1 3LE, Durham, UK. ³School of Biological and Biomedical Sciences, Durham University, South Road, Durham, DH1 3LE, UK, current address: Department of Molecular Biology and Biotechnology, University of Sheffield, Firth Court, Western Bank, S10 2TN, Sheffield, UK.

References

- Boogerd, F.C., Bruggeman, F., Hofmeyr, J.H.S., Westerhoff, H.V. (eds.): *Systems Biology Philosophical Foundations*. Elsevier, Amsterdam (2007)
- Alves, R., Antunes, F., Salvador, A.: Tools for kinetic modeling of biochemical networks. *Nat Biotech* **24**(6), 667–672 (2006)
- Jamshidi, N., Palsson, B.Ø.: Formulating genome-scale kinetic models in the post-genome era. *Molecular Systems Biology* **4**(171) (2008)
- Smallbone, K., Simeonidis, E., Swainston, N., Mendes, P.: Towards a genome-scale kinetic model of cellular metabolism. *BMC Systems Biology* **4**(6) (2010)
- Moore, S., Zhang, X., Mudge, A., Rowe, J.H., Topping, J.F., Liu, J., Lindsey, K.: Spatiotemporal modelling of hormonal crosstalk explains the level and patterning of hormones and gene expression in *Arabidopsis thaliana* wild-type and mutant roots. *New Phytologist* **207**(4), 1110–1122 (2015). doi:10.1111/nph.13421. 2015-19023
- Vernon, I., Goldstein, M., Bower, R.G.: Galaxy formation: a bayesian uncertainty analysis. *Bayesian Analysis* **5**(4), 619–670 (2010)
- Vernon, I., Goldstein, M., Bower, R.G.: Galaxy formation: Bayesian history matching for the observable universe. *Statistical Science* **29**(1), 81–90 (2014)
- Craig, P.S., Goldstein, M., Seheult, A.H., Smith, J.A.: Pressure matching for hydrocarbon reservoirs: a case study in the use of bayes linear strategies for large computer experiments (with discussion). In: Gatsonis, C., Hodges, J.S., Kass, R.E., McCulloch, R., Rossi, P., Singpurwalla, N.D. (eds.) *Case Studies in Bayesian Statistics* vol. 3, pp. 36–93. Springer, New York (1997)
- Kennedy, M.C., O'Hagan, A.: Bayesian calibration of computer models. *Journal of the Royal Statistical Society, Series B* **63**(3), 425–464 (2001)
- O'Hagan, A.: Bayesian analysis of computer code outputs: A tutorial. *Reliability Engineering and System Safety* **91**, 1290–1300 (2006)
- Andrianakis, I., Vernon, I., McCreech, N., McKinley, T.J., Oakley, J.E., Nsubuga, R., Goldstein, M., White, R.G.: Bayesian history matching of complex infectious disease models using emulation: A tutorial and a case study on HIV in Uganda. *PLoS Comput Biol.* **11**(1), 1003968 (2015)
- Williamson, D., Goldstein, M., Allison, L., Blaker, A., Challenor, P., Jackson, L., Yamazaki, K.: History matching for exploring and reducing climate model parameter space using observations and a large perturbed physics ensemble. *Climate Dynamics* **41**(7–8), 1703–1729 (2013)

13. Heitmann, K., Higdon, D., *et al.*: The coyote universe ii: Cosmological models and precision emulation of the nonlinear matter power spectrum. *Astrophys. J.* **705**(1), 156–174 (2009)
14. Oakley, J., O'Hagan, A.: Bayesian inference for the uncertainty distribution of computer model outputs. *Biometrika* **89**(4), 769–784 (2002)
15. Vernon, I., Goldstein, M., Bower, R.G.: Rejoinder for Galaxy formation: a bayesian uncertainty analysis. *Bayesian Analysis* **5**(4), 697–708 (2010)
16. Goldstein, M., Seheult, A., Vernon, I.: Assessing Model Adequacy. In: Wainwright, J., Mulligan, M. (eds.) *Environmental Modelling: Finding Simplicity in Complexity*, 2nd edn. John Wiley & Sons, Ltd, Chichester, UK (2013). doi:[10.1002/9781118351475.ch26](https://doi.org/10.1002/9781118351475.ch26)
17. Brynjarsdottir, J., O'Hagan, A.: Learning about physical parameters: The importance of model discrepancy. *Inverse Problems* **30**(114007), 24 (2014)
18. Goldstein, M., Rougier, J.C.: Reified bayesian modelling and inference for physical systems (with discussion). *Journal of Statistical Planning and Inference* **139**(3), 1221–1239 (2009)
19. Higdon, D., Kennedy, M., Cavendish, J.C., Cafoe, J.A., Ryne, R.D.: Combining field data and computer simulations for calibration and prediction. *SIAM Journal on Scientific Computing* **26**(2), 448–466 (2004)
20. Henderson, D.A., Boys, R.J., Krishnan, K.J., Lawless, C., Wilkinson, D.J.: Bayesian emulation and calibration of a stochastic computer model of mitochondrial dna deletions in substantia nigra neurons. *Journal of the American Statistical Association* **104**(485), 76–87 (2009)
21. Zamora-Sillero, E., Hafner, M., Ibig, A., Stelling, J., Wagner, A.: Efficient characterization of high-dimensional parameter spaces for systems biology. *BMC Systems Biology* **5**(1), 1–22 (2011). doi:[10.1186/1752-0509-5-142](https://doi.org/10.1186/1752-0509-5-142)
22. Bower, R.G., Vernon, I., Goldstein, M., Benson, A.J., Lacey, C.G., Baugh, C.M., Cole, S., Frenk, C.S.: The parameter space of galaxy formation. *Mon.Not.Roy.Astron.Soc.* **96**(454), 717–729 (2010)
23. Vernon, I., Goldstein, M.: Bayes linear analysis of imprecision in computer models, with application to understanding galaxy formation. In: Augustin, T., Coolen, F.P.A., Moral, S., Troffaes, M.C.M. (eds.) *ISIPTA'09: Proceedings of the Sixth International Symposium on Imprecise Probability: Theories and Applications*, pp. 441–450. SIPTA, Durham, UK (2009)
24. Rodrigues, L.F.S., Vernon, I., Bower, R.G.: Constraints to galaxy formation models using the galaxy stellar mass function, stronger feedback during starbursts? In Preparation (2016)
25. Andrianakis, I., Vernon, I., McCreesh, N., McKinley, T.J., Oakley, J.E., Nsubuga, R., Goldstein, M., White, R.G.: History matching of complex stochastic computer models using variance emulation, with application to an epidemiology model of hiv transmission. *RSSC in submission* (2016)
26. Craig, P.S., Goldstein, M., Seheult, A.H., Smith, J.A.: Bayes linear strategies for history matching of hydrocarbon reservoirs. In: Bernardo, J.M., Berger, J.O., Dawid, A.P., Smith, A.F.M. (eds.) *Bayesian Statistics 5*, pp. 69–95. Clarendon Press, Oxford, UK (1996)
27. Cumming, J.A., Goldstein, M.: Bayes linear uncertainty analysis for oil reservoirs based on multiscale computer experiments. In: O'Hagan, A., West, M. (eds.) *Handbook of Bayesian Analysis*. Oxford University Press, Oxford, UK (2009)
28. Cumming, J.A., Goldstein, M.: Small sample bayesian designs for complex high-dimensional models based on information gained using fast approximations. *Technometrics* **51**(4), 377–388 (2009)
29. Liu, J., Mehdi, S., Topping, J., Tarkowski, P., Lindsey, K.: Modelling and experimental analysis of hormonal crosstalk in arabidopsis. *Molecular Systems Biology* **6**(1), 373 (2010). doi:[10.1038/msb.2010.26](https://doi.org/10.1038/msb.2010.26). <http://msb.embopress.org/content/6/1/373.full.pdf>
30. Casson, S.A., Chilly, P.M., Topping, J.F., Evans, I.M., Souter, M.A., Lindsey, K.: The polaris gene of arabidopsis encodes a predicted peptide required for correct root growth and leaf vascular patterning. *The Plant Cell* **14**(8), 1705–1721 (2002)
31. Chilly, P.M., Casson, S.A., Tarkowski, P., Hawkins, N., Wang, K.L.C., Hussey, P.J., Beale, M., Ecker, J.R., Sandberg, G.K., Lindsey, K.: The polaris peptide of arabidopsis regulates auxin transport and root growth via effects on ethylene signaling. *The Plant Cell* **18**(11), 3058–3072 (2006)
32. Craig, P.S., Goldstein, M., Rougier, J.C., Seheult, A.H.: Bayesian forecasting for complex systems using computer simulators. *Journal of the American Statistical Association* **96**(454), 717–729 (2001)
33. Sacks, J., Welch, W.J., Mitchell, T.J., Wynn, H.P.: Design and analysis of computer experiments. *Statistical Science* **4**(4), 409–435 (1989)
34. Santner, T.J., Williams, B.J., Notz, W.I.: *The Design and Analysis of Computer Experiments*. Springer, New York (2003)
35. Currin, C., Mitchell, T., Morris, M., Ylvisaker, D.: Bayesian prediction of deterministic functions with applications to the design and analysis of computer experiments. *Journal of the American Statistical Association* **86**(416), 953–963 (1991)
36. Team, R.C.: *R: A Language and Environment for Statistical Computing*. R Foundation for Statistical Computing, Vienna, Austria (2015). R Foundation for Statistical Computing. <http://www.R-project.org/>
37. Goldstein, M.: Bayes linear analysis. In: Kotz, S., *et al.*(eds.) *Encyclopaedia of Statistical Sciences*, pp. 29–34. Wiley, ??? (1999)
38. Goldstein, M., Wooff, D.A.: *Bayes Linear Statistics: Theory and Methods*. Wiley, Chichester (2007)
39. Bastos, T.S., O'Hagan, A.: Diagnostics for gaussian process emulators. *Technometrics* **51**, 425–438 (2008)
40. Rougier, J.C.: Efficient emulators for multivariate deterministic functions. *Journal of Computational and Graphical Statistics* **17**(4), 827–843 (2008)
41. Vernon, I., Goldstein, M., Liu, J., Lindsey, K., Rowe, J.: Bayesian experimental design for physical systems modelled by computer simulators. In Preparation (2016)
42. Vernon, I., Goldstein, M., Liu, J., Lindsey, K., Rowe, J., Topping, J.: Bayesian experimental design for global parameter discovery with application to arabidopsis. In Preparation (2016)
43. Pukelsheim, F.: The three sigma rule. *The American Statistician* **48**, 88–91 (1994)
44. Wilkinson, D.J.: *Stochastic Modelling for Systems Biology*. Chapman and Hall, Taylor and Francis Group, LLC (2006)
45. Vanneste, S., Friml, J.: Auxin: a trigger for change in plant development. *Cell* **136**(6), 1005–1016 (2009). doi:[10.1016/j.cell.2009.03.001](https://doi.org/10.1016/j.cell.2009.03.001)
46. Friml, J., Benková, E., Blilou, I., Wisniewska, J., Hamann, T., Ljung, K., Woody, S., Sandberg, G., Scheres, B., Jürgens, G., Palme, K.: Atpin4 mediates sink-driven auxin gradients and root patterning in arabidopsis. *Cell* **108**(5), 661–673 (2002). doi:[10.1016/S0092-8674\(02\)00656-6](https://doi.org/10.1016/S0092-8674(02)00656-6)
47. Sabatini, S., Beis, D., Wolkenfelt, H., Murfett, J., Guilfoyle, T., Malamy, J., Benfey, P., Leyser, O., Bechtold, N., Weisbeek, P., Scheres, B.: An auxin-dependent distal organizer of pattern and polarity in the arabidopsis root. *Cell* **99**(5), 463–472 (1999). doi:[10.1016/S0092-8674\(00\)81535-4](https://doi.org/10.1016/S0092-8674(00)81535-4)
48. Garay-Arroyo, A., De La Paz Sánchez, M., García-Ponce, B., Azpeitia, E., Álvarez-Buylla, E.R.: Hormone symphony during root growth and development. *Developmental Dynamics* **241**(12), 1867–1885 (2012). doi:[10.1002/dvdy.23878](https://doi.org/10.1002/dvdy.23878)
49. Chaiwanon, J., Wang, W., Zhu, J.Y., Oh, E., Wang, Z.Y.: Information integration and communication in plant growth regulation. *Cell* **164**(6), 1257–68 (2016)
50. Liu, J., Mehdi, S., Topping, J., Friml, J., Lindsey, K.: Interaction of pl and pin and hormonal crosstalk in arabidopsis root development. *Frontiers in Plant Science* **4**(75) (2013). doi:[10.3389/fpls.2013.00075](https://doi.org/10.3389/fpls.2013.00075)
51. Lindsey, K., Rowe, J., Liu, J.: Hormonal crosstalk for root development: a combined experimental and modelling perspective. *Frontiers in Plant Science* **5**(116) (2014). doi:[10.3389/fpls.2014.00116](https://doi.org/10.3389/fpls.2014.00116)
52. Moore, S., Zhang, X., Liu, J., Lindsey, K.: *Modelling Plant Hormone Gradients*. eLS. John Wiley & Sons Ltd, Chichester (2015)
53. Rowe, J.H., Topping, J.F., Liu, J., Lindsey, K.: Abscisic acid regulates root growth under osmotic stress conditions via an interacting hormonal network with cytokinin, ethylene and auxin. *New Phytologist*, (2016). doi:[10.1111/nph.13882](https://doi.org/10.1111/nph.13882). 2015-20300